ARTICLE IN PRESS

Communications Earth & Environment https://doi.org/10.1038/s43247-026-03653-2

Article in Press

Gold mobility in subduction zones, the slab perspective

Received: 25 September 2025

Accepted: 12 May 2026

Cite this article as: Patten, C.G., Peillod, A., Hector, S. *et al.* Gold mobility in subduction zones, the slab perspective. *Commun Earth Environ* (2026). https://doi.org/10.1038/s43247-026-03653-2

Clifford G. C. Patten, Alexandre Peillod, Simon Hector, Barbara I. Kleine-Marshall, Aratz Beranoaguirre, Antonin Bilau, Kirsten Drüppel, Jesse B. Walters, Iain Pitcairn, Uwe Ring, Alasdair Skelton & Jochen Kolb

We are providing an unedited version of this manuscript to give early access to its findings. Before final publication, the manuscript will undergo further editing. Please note there may be errors present which affect the content, and all legal disclaimers apply.

If this paper is publishing under a Transparent Peer Review model then Peer Review reports will publish with the final article.

ARTICLE IN PRESS

© The Author(s) 2026. **Open Access** This article is licensed under a Creative Commons Attribution 4.0 International License, which permits use, sharing, adaptation, distribution and reproduction in any medium or format, as long as you give appropriate credit to the original author(s) and the source, provide a link to the Creative Commons licence, and indicate if changes were made. The images or other third party material in this article are included in the article's Creative Commons licence, unless indicated otherwise in a credit line to the material. If material is not included in the article's Creative Commons licence and your intended use is not permitted by statutory regulation or exceeds the permitted use, you will need to obtain permission directly from the copyright holder. To view a copy of this licence, visit http://creativecommons.org/licenses/by/4.0/.

ARTICLE IN PRESS

Gold mobility in subduction zones, the slab perspective

Clifford G.C. Patten[1,2*], Alexandre Peillod[2], Simon Hector[2], Barbara I. Kleine-Marshall[3], Aratz Beranoaguirre[4], Antonin Bilau[2], Kirsten Drüppel[2], Jesse B. Walters[5], Iain Pitcairn[6], Uwe Ring[6], Alasdair Skelton[6], Jochen Kolb[2]

[1]Institute of Mineralogy and Petrography, University of Innsbruck, Innsbruck, Austria *clifford.patten@uibk.ac.at

[2]Chair for Economic Geology and Geochemistry, Institute of Applied Geosciences, Karlsruhe Institute of Technology, Karlsruhe, Germany

[3]GeoZentrum Nordbayern, Department of Geography and Geosciences, Friedrich-Alexander University, Erlangen-Nuremberg, Germany

[4]Institut für Geowissenschaften, Goethe-Universität Frankfurt, Frankfurt, Germany

[5]Department of Earth Sciences-NAWI Graz Geocenter, University of Graz, Graz, Austrian

[6]Department of Geological Sciences, Stockholm University, Stockholm, Sweden

Abstract

Arc environments are locally gold-endowed and it has been long hypothesized that gold mobilization during slab dehydration could affect mantle composition and arc Au-fertility. Here, we determine gold mobility during prograde high pressure-low temperature metamorphism of both metavolcanic and metasedimentary rocks from the islands of Santorini, Ios, Naxos and Syros (Greece). These rocks experienced peak greenschist to upper-blueschist/eclogite facies metamorphism, allowing determination of large-scale gold mobility within a subduction zone. Our data shows that gold is significantly mobilized by fluids at the blueschist-eclogite facies transition. In the associated mélange zones at the slab-mantle interface gold shows heterogeneous concentration but is not enriched, implying only partial retention of gold in the mélange and its mobilization across the slab-mantle interface. Furthermore, the intrinsically complex lithologies and heterogenous gold concentrations of these mélange zones contribute to the slab component inherent to arc magmatism, and can affect magmatism gold-fertility.

ARTICLE IN PRESS

ARTICLE IN PRESS

Introduction

Fluid fluxes in subduction zones promote the transfer of elements from the altered oceanic crust and sediments to the overlying mantle. These fluxes affect the mantle composition and its redox budget, having a profound impact on arc environments (*1*–*4*). Arcs are favorable geological settings for the formation of major magmatic-hydrothermal ore deposits variably enriched in Au, such as porphyry, skarn, epithermal and volcanogenic massive sulfide, as well as orogenic Au deposits during arc accretion (*5*–*10*). Gold enrichment in the mantle has been suggested as a prerequisite for the formation of some Au-rich deposits (*11*–*14*), but this process is not systematic and the metasomatized mantle can either be locally Au-enriched (*11*, *13*, *15*) or barren (*16*, *17*). Overall, the mobility of Au during slab dehydration, slab-mantle interaction and mantle melting, as well as its impact on ore deposit formation, has been extensively discussed but has not yet been tested from the slab perspective.

Conversely, mobility of Au during Barrovian metamorphism is fairly well understood, where devolatilization during prograde metamorphism at upper amphibolite metamorphic facies conditions effectively generates metamorphic H_2O-CO_2 fluids capable of transporting Au (*6*, *18*). Gold is most efficiently mobilized at ~550 °C and is sourced from both metasedimentary and metavolcanic rocks (*19*–*21*). High pressure-low temperature (HP-LT) metamorphism in subduction zones shares broad similarities with Barrovian metamorphism, albeit at different pressure and redox conditions. Prograde HP-LT metamorphism leads to progressive devolatilization of H_2O, CO_2 and other volatiles from the descending slab into the overlying mantle wedge, promoting mantle metasomatism, melting and arc magmatism (*22*).

This study investigates the mobilization of Au during prograde HP-LT metamorphism of the Cycladic Blueschist Unit (CBU). The CBU, within the Hellenide orogen in Greece, records a complex but coherent prograde P-T path from greenschist (~300 °C; ~7 kbar) to upper-blueschist/eclogite facies (~550 °C; ~22 kbar) recorded by rocks from the islands of Santorini, Ios, Naxos and Syros. To gain a comprehensive understanding of Au-mobility in a subduction zone, Au is investigated for both metavolcanic and metasedimentary rocks from the subducted and now obducted slab, as well as from mélange zone rocks, representing the slab-mantle interface. The results show that Au is significantly mobilized during prograde

ARTICLE IN PRESS

ARTICLE IN PRESS

HP-LT metamorphism, revealing significant Au fluxes in subduction zones and Au cycling in arc systems.

Results

Geological settings

The study area is the Cycladic zone of the Hellenide orogen. The Cycladic zone consists of fragments of the northern passive continental margin of the Adriatic plate and remnants of a subducted oceanic crust (Figure 1). Within the Cycladic zone, the CBU represents the most deeply exhumed part of the Hellenides. In simplified term, the CBU is subdivided into three separate members: (a) the Bottom-CBU nappe, a Carboniferous basement; (b) the Middle-CBU nappe, a Permo-Carboniferous to late Cretaceous sequence of alternating metasedimentary and metavolcanic rocks; and (c) the Top-CBU nappe, an ophiolite-like mélange zone representing a distal continental margin and an oceanic slab assembled in a slab mélange zone (*23–25*) (Figure 1).

Three main tectono-metamorphic stages of the Middle-CBU nappe are distinguished: a) Eocene/Oligocene HP metamorphism during subduction, b) Eocene/Oligocene early exhumation to mid-crustal depths and retrograde greenschist facies metamorphism, and c) exhumation from the mid-crust to the surface, associated with slab-roll back and low-angle detachment faulting during the Miocene (*26–28*). The P-T conditions estimated for peak metamorphism vary significantly. In Santorini, they are ~7.6 kbar and ~330 °C (upper-greenschist facies) (*26*, *29*), ~13 kbar and ~500 °C in Ios (lower-blueschist facies) (*26*, *30*), ~16 kbar and 575 °C in Naxos (upper-blueschist facies, South-Naxos) (*31*) and 19-24 kbar and 500-575°C in Syros (upper blueschist/eclogite facies transition) (*32*, *33*). Despite various exhumation mechanisms many rocks preserved their peak metamorphism parageneses. The Top-CBU nappe at Syros shows similar peak P-T conditions like the Middle-CBU nappe but has sustained local retrogression from eclogite to greenschist facies (*24*, *34*). The petrographic overview of the Middle- and Top-CBU is provided in the supplementary note 1 (Supplementary Figure 1-5) and in the supplementary data 1.

Gold content of metavolcanic rocks

The metavolcanic rocks from the Middle-CBU nappe on Santorini, Ios, Naxos and Syros have an overall arc affinity (*35*) (Supplementary Note 2 and Supplementary Figure 6). They

ARTICLE IN PRESS

show, however, large chemical variations, from tholeiitic, mainly on Ios and Naxos, to calc-alkaline, mainly on Santorini and Syros (Supplementary Figure 6c), representative of the lithological diversity in passive margin sequences (*25*) and preventing straightforward classification to a specific magmatic setting. Melt contamination by subduction fluids/melts (slab component) and crustal material can account for such diversity (Supplementary Figure 6d) and is highlighted by progressive light rare earth element enrichment (Supplementary Figure 7a-b). Such geochemical signatures have similarities with modern-day supra-subduction arc analogues (Supplementary Figure 6). Greenschist to upper-blueschist facies metavolcanic rocks from the Middle-CBU nappe at Santorini (n=7), Ios (n=14) and Naxos (n=7) have similar Au concentrations with median values of 0.88 ng.g^{-1}, 0.84 ng.g^{-1} and 0.94 ng.g^{-1}, respectively, whereas blueschist-eclogite facies transition rocks from Syros (n=14) have a lower median Au concentration of 0.28 ng.g^{-1} (Figure 2, Table 1).

The Top-CBU nappe at Syros consist of large, massive metavolcanic blocks in a chlorite-talc schist matrix forming a mélange zone (*24*, *36*). The blocks have tholeiitic affinity with complex REE patterns (Supplementary Figure 6-7) whereas the matrix corresponds to variably metasomatized ultramafic rocks (*24*) (Supplementary Figure 7). The mélange zone has an overall Au median of 0.72 ng.g^{-1} (Figure 2). The blocks have a median Au concentration of 0.86 ng.g^{-1} (n=14) ranging between 0.30 and 6.21 ng.g^{-1} and the matrix has a median Au concentration of 0.57 ng.g^{-1} (n=10), ranging between 0.23 and 6.99 ng.g^{-1} (Figure 2, Table 1).

ARTICLE IN PRESS

Gold content of metasedimentary rocks

The bulk of the Middle-CBU nappe consists of metasedimentary rocks. The siliceous metasedimentary rocks are dominated by metapsammite with minor metapelite and rare quartzite (Supplementary Figure 6e). The immobile element contents of metapsammites and metapelites suggest an oceanic island arc to continental arc affinity (Supplementary Figure 6f). Their Au concentration ranges from 0.07 ng.g-1 up to 418 ng.g^{-1} with a median of 0.78 ng.g^{-1} (n=65). Median Au concentration is 0.80 ng.g^{-1} for samples metamorphosed at greenschist facies (Santorini, n=12), 1.12 ng.g^{-1} for those at lower-blueschist facies (Ios, n=21), 1.69 ng.g^{-1} for those at upper-blueschist facies (Naxos, n=22) and 0.29 ng.g^{-1} for those at the blueschist/eclogite facies transition (Syros, n=6, Figure 2, Table 1). Two quartzite samples have 0.42 and 0.47 ng.g^{-1} Au and two marbles have 0.28 and 0.23 ng.g^{-1} Au, respectively (Supplementary Data 1).

Content of volatiles, As and Sb in metavolcanic and metasedimentary rocks

Gold is often mobilized alongside volatiles, mainly H_2O and CO_2 inferred from the loss on ignition (LOI), and other elements during Barrovian metamorphism such as S, As and Sb (*19*, *37*). For metavolcanic rocks from the Santorini, Ios, Naxos, Syros Middle-CBU and Syros Top-CBU, LOI median concentrations are 4.91, 3.75, 2.43, 3.81 and 2.37 wt.%, S median concentrations are 100, 60, 120, 180 and 205 μg.g^{-1}, As median concentrations are 3.16, 0.98, 0.73, 0.37 and 0.83 μg.g^{-1}, and Sb median concentrations are 0.65, 0.40, 0.51, 0.12 and 0.12 μg.g^{-1}, respectively; correlating with increasing grades of metamorphism (3a, Supplementary Data 1). In the corresponding metasedimentary rocks, LOI median concentrations are 8.89, 4.30, 3.64 and 3.03 wt.%, S median concentrations are 85, 60, 141 and 130 μg.g^{-1}, As median concentrations are 17.5, 1.50, 1.79 and 0.54 μg.g^{-1} and Sb median concentrations are 0.72, 0.44, 0.99 and 0.09 μg.g^{-1} in Santorini, Ios, Naxos and Syros Middle-CBU, respectively (Figure 3b, Supplementary Data 1).

Discussion

Gold mobility during prograde HP-LT metamorphism

Gold mobility during prograde HP-LT metamorphism is determined using only samples from the Middle-CBU nappe, which was subducted as a coherent nappe during the Eocene (*26*). Importantly, samples from Syros Top-CBU are not considered for determining Au mobility during prograde HP-LT metamorphism. To determine Au mobility the Au concentration and distribution in metamorphic protoliths needs to be first determined, especially for metavolcanic rocks which is challenging *(21)*. The metavolcanic rocks from Santorini and Syros Middle-CBU show calc-alkaline affinity while those from Ios and Naxos Middle-CBU show tholeiitic to transitional affinity, implying protoliths with possibly different Au content at the onset of metamorphism. Fortunately, the tholeiitic metavolcanic rocks from Ios and Naxos show supra-subduction zone (SSZ) affinity similarly to those of Santorini and Syros (Supplementary Figure 6). The SSZ affinity of the CBU passive margin metavolcanic rocks (*38*, *39*) implies a complex, but similar Au distribution within the protoliths for all localities before metamorphism. Gold behavior during magmatic differentiation in a SSZ environment is strikingly different from mid-oceanic ridge basalts

ARTICLE IN PRESS

(MORB) and depends on numerous parameters such as melt composition, redox condition, volatile content and, importantly, the timing of sulfide saturation and volatile degassing (*40*, *41*). In many SSZ localities, Au behaves as an incompatible element during the early stage of magmatic differentiation, usually because the melt is sulfide undersaturated. In the late stage of differentiation, however, its behavior changes to strongly compatible due to sulfide saturation and/or magmatic degassing, leading to a strong drop in the Au content usually concomitant with the onset of advanced magnetite crystallization (*42–46*) (Figure 4a). Hence, the SSZ affinity of the volcanic rocks exerts a first order control on the protolith Au content and distribution prior post-magmatic processes.

To define Au distribution in the metavolcanic rock protoliths we assessed Au concentration relative to MgO and V. Although MgO is a commonly used proxy for magmatic differentiation it can be partly affected by hydrothermal seafloor alteration. Commonly used immobile elements, such as Zr and Y, do not work properly for the Middle-CBU nappe sample set, as some samples show high Y and Zr concentrations possibly due to the presence of accessory minerals such as zircon or apatite. Vanadium is used instead as a proxy for the overall magmatic differentiation (Figure 4b-c). It behaves in a similar way as Au during magmatic differentiation (Figure 4b), although not being controlled by the same phases, and is relatively immobile during seafloor alteration and metamorphism. The Au/Cu ratio is also useful to decipher Au distribution within the metavolcanic protolith (Figure 4c). Copper, being a strongly chalcophile element, behaves similarly to Au during magmatic differentiation in SSZ environments (*42*, *44–46*). This is highlighted by the overall constant Au/Cu ratio in diverse SSZ analogues during differentiation, ranging within one order of magnitude (Figure 4c). Additionally, Cu is less mobile than Au during seafloor alteration and Barrovian metamorphism, although not being fully immobile (*37*, *47*).

The samples from Santorini, Ios and Naxos, do not show a Au distribution which can be related to magmatic differentiation but the Au concentrations plot within the range of the SSZ analogues (Figure 4a-c). This is likely due to post-magmatic Au remobilization, possibly during seafloor alteration (*47*). Gold concentrations in samples from Syros Middle-CBU nappe, however, do not overlap with those of samples from the other localities nor with SSZ analogues, showing that the low Au concentration in rocks metamorphosed at the upper-blueschist/eclogite facies transition is not related to magmatic processes.

ARTICLE IN PRESS

ARTICLE IN PRESS

Variations in Au content relative to MgO and V in metavolcanic rocks from the Middle-CBU nappe during prograde HP-LT metamorphism provides better insight into Au mobility (Figure 5). The MgO and V content of metavolcanic rocks show no noticeable variation related to metamorphic grade while Au/MgO and Au/V show pronounced decrease in value at the upper blueschist-eclogite transition (Figure 5). This indicates that the decrease in Au at the upper blueschist/eclogite metamorphic grade (Figure 2) is not due to differences in the initial protolith composition otherwise both the Au/MgO and Au/V would have remained constant. This confirms further that the variations observed in Au concentrations are related to prograde metamorphic devolatilization rather than differences related to magmatic processes.

To truly determine Au mobility during HP-LT metamorphism, the Au content of the samples metamorphosed at the lowest metamorphic grade need to be used as a reference frame (*19*, *21*). Notably, low-grade metamorphic samples record the same pre-metamorphic history as their high-grade metamorphic counterparts, allowing comparison. The limited exposure of the Middle-CBU nappe at Santorini prevents building a large and comprehensive low-grade metamorphic sample suite which can be used as a metamorphic protolith. To circumvent the issue, the samples from Santorini (n=21) are paired with those from Ios (n=40). Peak metamorphic temperatures on Ios are ~470-500 °C (*26*), the upper limit at which Au is still not extensively mobilized from both metavolcanic and metasedimentary rocks during Barrovian metamorphism (*18*, *19*, *21*). The sample set from Santorini and Ios does not represent a true metamorphic protolith at the onset of metamorphism, but it is a proxy for the Au content in rocks metamorphosed at the upper greenschist-lower blueschist facies, allowing to determine if Au is mobilized at higher metamorphic grades. Mann-Whitney U statistical tests are performed to define if the Au content of rocks metamorphosed at upper greenschist-lower blueschist facies are statistically different from those metamorphosed at higher conditions (Table 2). Both metavolcanic and metasedimentary rocks from Syros Middle-CBU nappe, metamorphosed to upper blueschist-eclogite metamorphic facies transition, have significantly lower Au contents than those metamorphosed at the upper greenschist-lower blueschist facies, implying that Au mobilization does occur during prograde HP-LT metamorphism (Figure 2 and 5). This outcome is somehow similar to Au

ARTICLE IN PRESS

mobilization during Barrovian metamorphism when Au is significantly mobilized in the upper amphibolite facies (*19*).

Arsenic and Sb, which are generally mobilized alongside Au and enriched in orogenic Au deposits (*19*, *20*, *37*), also show decreasing concentrations in both metavolcanic and metasedimentary rocks from the Middle-CBU with increasing HP-LT metamorphism (Figure 3), implying similar mobilization to Au. Sulfur, on the other hand, shows increasing concentrations in both metavolcanic and metasedimentary rocks with increasing HP-LT metamorphism (Figure 3), which is the opposite of its behavior during Barrovian metamorphism (*18*). While the S behavior during Barrovian metamorphism is mainly controlled by the pyrrhotite-pyrite mineral reaction (*18*, *19*), S mobility in HP-LT metamorphism is more complex, associated with various S species sensitive to redox and complex mineral reactions (*36*, *48*, *49*).

Where does the Au go?

The fluids released during HP-LT metamorphism migrate towards the slab-mantle interface (*3*). They are generally H_2O-dominated with variable C species (CO_2-CH_4) and diverse salinity (*50*, *51*), similar to Barrovian metamorphic fluids (*52*) except possibly for their redox conditions. When the HP-LT metamorphic fluids reach and migrate along the slab-mantle interface, their redox budget depends on the content of redox-sensitive species, pathways and on fluid-rock ratios, resulting in an overall heterogenous system (*53*). These processes will alter the speciation of Aug ligands and influence Au solubility and transport.

Gold transport in fluids is generally by hydrogen sulfide or chlorine complexes, but oxidizing conditions do not promote Au mobilization by hydrogen sulfide complexes (*54*, *55*). The variable salinity of the HP-LT metamorphic fluids (from 4 to >20 wt.% NaCl) (*50*) and Cl devolatilization during prograde metamorphism (*56*) could promote Au transport as chlorine complex. Despite the variable redox conditions of HP-LT metamorphic fluids, the diversity of Au complexes stable over relatively wide range of P-T and redox conditions (*57*) allows for Au transport in HP-LT metamorphic fluids.

Gold in the mélange zone at the slab-mantle interface

Mélange zones are characterized by physical mixing as well as advective and diffusive metasomatism between diverse lithologies, mainly ultramafic, metavolcanic and

ARTICLE IN PRESS

ARTICLE IN PRESS

metasedimentary rocks at the slab-mantle interface (*24*, *58*, *59*). The mélange zone at Syros Top-CBU nappe records such complex processes during both prograde and protracted retrograde metamorphism from eclogite to greenschist facies, in particular associated with fluid flow over a wide P-T range at the slab-mantle interface (*24*). The Au content in the mélange zone at Syros is not specifically associated with either a sedimentary, altered oceanic crust or mantle component (Figure 6a). Instead, its large Au variability (Figure 2) reflects local enrichment of Au in both the metavolcanic blocks and the schist matrix; sometimes metasomatic sulfides are present at the contact between the two, likely due to local redox changes (*36*) (Au>3 ng.g^{-1}, n=7; Supplementary Figure 6). Metasomatic sulfides in the mélange zone most likely exert a strong control on Au distribution as they are the main mineral host for most chalcophile elements (*60*). Most of the samples, however, have Au concentrations below 1 ng.g^{-1} (n=13; Supplementary Data 1). The overall low Au content of the mélange zone (median = 0.72 ng.g^{-1}) relative to the modern lithospheric mantle (Au median = 1.2 ng.g^{-1}, 0.6-2.2 ng.g^{-1}) or the primitive mantle (Au median = 1.4 ng.g^{-1}, 0.8-2.0 ng.g^{-1}) (*16*) implies that the Au released from the slab by HP-LT metamorphic fluids is not enriched in the mélange zone, despite local enrichment, but is rather transported elsewhere with the fluids.

Gold transport to the mantle and the crust

Fluid flow at slab-mantle interface depends on lithology, mineralogy, temperature, permeability, rheology, and compaction pressure (*61–64*). The majority of the fluids tend to travel upslope along the slab-mantle interface (*64*) although some can partly migrate within the mantle wedge (*62*) (Figure 7). The apparent lack of Au enrichment in the mélange zone at Syros Top-CBU indicates that Au is efficiently mobilized along the slab-mantle interface as it was not enriched during retrograde metamorphism.

The Au mobilized upwards along the slab-mantle interface may be integrated into the hydrothermal system of the overriding crust where Barrovian metamorphism occurs and some orogenic Au deposits may form (*5*, *52*) (Figure 7). For instance, Au enrichment in the forearc mantle during low-temperature metasomatism (<300 °C-400 °C) has been reported to be associated with lizardite-antigorite serpentinization and mantle-derived CO_2-H_2O-rich fluids (*15*); possibly representing the shallow path of Au-rich fluids originating deeper within the subduction zone. Alternatively, fluid migration within the mantle wedge, rather than

ARTICLE IN PRESS

along the slab-mantle interface, is anticipated to form metasomatized mantle domains with high or heterogeneous Au content, often referred to as fertile sub-continental lithospheric mantle (Figure 7). Later, these can be involved in the formation of post-subduction orogenic Au and Au-rich magmatic-hydrothermal deposits (*12–14*, *65*).

Gold and arc magmatism

While fluids travel upwards along the slab-mantle interface, the hydrated and mechanically weak metasomatized rocks are dragged to depth by the subducting slab, leading to decoupling between fluids and rocks. Although the mechanisms for crustal material transfer within the mantle wedge are debated (*58*, *66–72*), the contribution of a slab component to arc magmatism is accepted (*58*, *67*). On initiation of melting, either at slab surface or in a rising diapir (*58*), the mélange zone is most likely not Au-depleted as some Au is concentrated in the heterogeneously distributed metasomatic sulfides which are stable until high PT conditions (*73*). Melting of mélange zones will thus lead to a notably different geochemical signature for Au compared to melting of depleted or metasomatized mantle (Figure 7). This process may directly recycle the Au retained in the mélange zones into arc magmas. Therefore, the strongly heterogeneous Au distribution and abundance of metasomatic sulfides in the mélange zone, mainly pyrite, chalcopyrite and bornite (*36*), likely play an important role for the timing of Au release during melting (*74*).

The relative proportion and nature of rock types within mélange zones, and their metamorphic and metasomatic evolution prior to melting dictate the slabs´ geochemical signature in arc magmas (*58*), implying a potential relationship between the slab component and Au-fertility of arc magmas (Figure 6a). For example, arc volcanic rocks with high Ba/Th but low La/Sm_n ratios, due to a slab component buffered by altered oceanic crust (*58*) or pelagic sediments (*75*) show a noticeably high Au content (Figure 6b-d; Manus Basin, median Au = 5.5 $ng.g^{-1}$; Kermadec arc median Au = 5.5 $ng.g^{-1}$). On the other hand, volcanic arcs showing high La/Sm_n but low Ba/Th ratios, due to a slab component buffered by terrigenous sediments (*58*, *75*) have distinctively lower Au contents (Christiana-Santorini-Kolumbo volcanic field median Au = 0.8 $ng.g^{-1}$; Eolian arc median Au = 0.1 $ng.g^{-1}$; Figure 6b-d). Overall, a positive correlation (R^2=0.43) is observed for Au and Ba/Th in relatively primitive volcanic arc rocks (i.e. before onset of sulfide or volatile saturation, Supplementary Data 6, Figure 6b) while a negative correlation (R^2=0.49) is observed for Au and La/Sm_n in

ARTICLE IN PRESS

these suites, where volcanic rocks with high La/Sm$_n$ (~>3) show noticeably low Au concentrations (0.1-0.3 ppb Au, Figure 6c). The nature of the slab component, therefore, can affect primitive arc magma Au-fertility (Figure 6b-d). Specifically, the nature of the subducted sediments is likely critical as pelagic sediments, such as black shales, can have high Au content (*76*) while terrigenous sediments can lead to Au-barren melt.

Implications for Au-rich deposits in arc settings

The formation of Au-rich deposits in arc environments, such as porphyry, epithermal, skarn and volcanogenic massive sulfide, is associated with diverse magmatic-hydrothermal processes occurring in the mid to shallow crust. Deposit formation depends, for example, on volatile degassing, timing of sulfide saturation, sulfide transport and oxidation, style of magmatism, crustal thickness, and longevity of magma reservoirs (*77–82*). The role of the mantle source and the magma Au-fertility has long been debated but is generally considered secondary to processes at shallow crustal depths. The evolution of the Hellenic subduction system over the last 50 Ma provides insight into the relationship between mélange zones, magma Au-fertility and Au-rich deposits.

ARTICLE IN PRESS

During the evolution of the Aegean arc since the Eocene, porphyry and epithermal Au-rich deposits mainly formed between 37-20 Ma in the Rhodopes and Biga areas, and after ~2 Ma in the South Aegean Volcanic Arc, such as in Milos and Kolumbo (*83–86*) (Figure 8). In between these two periods a hiatus in Au-rich deposit formation occurred. Concomitantly, the style of magmatism of the Aegean arc changed between 35 to 5 Ma from calc-alkaline to high-K and shoshonitic affinities and volcanic rocks show variations in slab component signature (*66*) (Figure 8-9). From ~35 to 20 Ma the slab component recorded in volcanic rocks shows an increase in (La/Sm)$_n$ up to ~5-6 while Ba/Th records a relatively constant value between ~60-100 (Figure 8), indicating an increase in the terrigenous component affecting the slab signature. Between 20 to 2 Ma, the (La/Sm)$_n$ remains elevated, with values between 4-6, while Ba/Th still remains between ~60-100 (Figure 8). The overall high (La/Sm)$_n$ over this period is associated with a slab component increasingly and steadily dominated by continental-derived terrigenous sediments (*66*). Since 2 Ma, a decrease in (La/Sm)$_n$ and Sr isotope values as well as a switch in magmatism back to calc-alkaline affinity (*66*) indicates a slab component progressively buffered back by altered oceanic crust and/or pelagic sediments at the expanse of terrigenous sediments (Figure 8-9) (*66*). The

ARTICLE IN PRESS

evolution of the slab component signature in the Hellenic arc has been attributed to diapirism (*66*), although this does not exclude contribution from slab melt and/or fluids (*87*). The intermediate geothermal gradient of the Hellenic subduction (~7-10 °C/Km; *2*, *26*) and the slab component signature varying between altered oceanic crust, mantle and terrigenous sediments suggest that diapirism could have occurred since the Eocene (*88*).

The variation in the style of magmatism and slab component signature between ~35 Ma to 5 Ma is caused by the onset of subduction of the Adriatic continental plate composed of the CBU and the external Hellenides since ~50 Ma (Tripolitza and Ionan blocks; Figure 8-9) (*28*, *66*, *89*). At ~50 Ma the Top-CBU nappe, corresponding to the distal passive margin of the Adriatic continental plate, reached peak metamorphism (Figure 8-9) and the associated mélange zone was dominated by an altered oceanic crust and/or pelagic sediment component as observed from the Top-CBU at Syros (Figure 6). Slab or diapir melting resulted in a melt with low $(La/Sm)_n$ and moderate Au-fertility (Figure 8). A lag of ~10-15 Ma between HP-LT metamorphism in the slab and magmatism in the arc is inferred from the tectonic evolution of the Hellenic subduction system (Figure 8) (*28*, *89*). Hence, melts generated from mélange zones associated with Top-CBU peak metamorphism can be related to volcanism at 40-35 Ma in the Rhodope and Biga areas and corresponding to the onset of Au-rich deposit formation (~37 Ma, Figure 8-9) (*83*).

Further subduction of the Adriatic passive margin, represented by the Middle-CBU with peak metamorphism at ~45-40 Ma (*26*, *90*), leads to changes in the mélange zone components, possibly a mixture between altered oceanic crust and/or pelagic sediments and terrigenous sediments. Slab or diapir melting resulted in melts with increasing La/Sm_n and lower Au-fertility. Such change is observed in volcanism between ~30-25 Ma where La/Sm_n is significantly increasing, yet Au-rich deposits are still forming (Figure 8) (*83*). This implies that the magma Au-fertility, at this stage, is not a first order factor controlling the formation of Au-rich deposits, but that mid to shallow crustal processes are more important. Specifically, at ~35-30 Ma magmatism switched to high-K affinity which is known to be associated with the formation of Au-rich porphyry and epithermal deposits (*91*) due to hydrothermal processes rather than magma Au-fertility (*79*).

At ~30 Ma, the Bottom-CBU reached peak metamorphism (Fig 7-8) followed by the external Hellenides at 25-20 Ma. The mélange zones formed from the subduction of these units was

ARTICLE IN PRESS

strongly dominated by a terrigenous component (*66*) which resulted, after melting, in melts with high La/Sm_n and very poor Au-fertility. Volcanism between 20 and 5 Ma is characterized by constantly high La/Sm_n (~>4, Figure 8) and no Au-rich deposit formation despite high-K magmatism. We infer that the long-lasting and strong buffering of slab components by terrigenous sediments ultimately led to magma Au-fertility so poor (e.g. ~0.1 ppb) that mid to shallow processes were not sufficient for Au-rich deposit formation over this period.

Following the Adriatic continental plate subduction, the subduction of the East Mediterranean oceanic plate at ~15 Ma resulted in a mélange zone buffered back by an altered oceanic crust and/or pelagic sediments. The resulting magma, from slab or diapir melting, had moderate Au-fertility, allowing the formation of Au-rich deposits via mid to shallow crustal processes since 2 Ma (Figure 8-9).

The 50 Ma evolution of the Hellenic subduction system highlights the interplay between source processes, i.e. the slab component effect on magma Au-fertility, and shallow to mid crustal processes, such high-K magmatism, on the formation of Au-rich ore deposits in the Aegean arc.

Materials and methods

A suite of 131 samples has been petrographically studied and analyzed for major and trace elements as well as for Au. To constrain Au-mobility during prograde HP-LT metamorphism sampling focused on rocks representative of local peak metamorphic conditions in the Middle-CBU nappe. Metamorphic facies were determined from mineral assemblages and PT calculations (*26*, *31*, *33*, *90*). Samples showing a minimum retrograde metamorphic overprint were selected and the sample suite has been checked for local metasomatism (e.g. Ca or Fe metasomatism). This was achieved by calculating alteration indexes (*92*) as well as checking for samples with non-coherent REE profiles. Classification of samples as metavolcanic or metasedimentary rocks was achieved by combining field petrography, optical microscopy, and chemical classification (*93*). Samples from Naxos are, as much as possible, from the southern part of the island, as the northern part underwent significant retrograde overprint (*31*).

ARTICLE IN PRESS

ARTICLE IN PRESS

Gold analysis

Gold analysis was done on pressed powder pellets (PPP) by laser ablation-inductively coupled plasma-mass spectrometry (LA-ICP-MS) using a Teledyne 193 nm Excimer Laser coupled to an Element XR ThermoFisher at the Laboratory for Environmental and Raw Materials Analysis (LERA), KIT, using ultra-low Au analysis method (*94*). Pressed-powder pellets were made by nano milling of sample rock powder using a Pulverisette 7 planetary mill (*94*, *95*). Pellet ablation was done with a laser beam diameter of 150 µm, a frequency of 100 Hz and a fluence of 5 J.cm^{-2}, optimized for Au sensitivity (*94*). Each pellet was analyzed 5 times. Measurements of Si^{29}, Ca^{44}, Hf^{180}, Ta^{181} and Au^{197} have been made for calibration and oxide interference corrections (*94*). Data reduction was done using the 3DRS plugin from IOLITE (*96*) using Si^{29} as the internal standard. Pellets of the reference materials TDB-1, BHVO-2, BCR-2, MRG-1 and UM-2 have been used for testing accuracy and precision (Supplementary Data 2). Analyses of TDB-1, a CanMet certified reference material and well-suited standard for low-Au analysis, has an accuracy of 6 % and a precision of 14.5 %. Other standards, not referenced for Au, have lower precision and accuracy but are in accordance published values (Supplementary Data 2). The method limit of detection (MLOD) is determined from repeated analyses of a Au-poor pellet and varies between runs (n=5) depending on the analytical conditions. The MLOD ranges between 0.07 and 0.24 ng.g^{-1}. Four samples have concentrations below the MLOD and are reported as the run MLOD value.

ARTICLE IN PRESS

Major and trace element analysis

Major element whole rock concentrations were analyzed by waverlength-dispersive X-ray fluorescence using a S4 Explorer Bruker AXS at LERA. The reference materials BHVO-1, MRG-1, AGV-1, RGM-1 and SY-2 were used for checking precision and accuracy (Supplementary Data 3). Trace element analyses were carried out by PPP-LA-ICP-MS (*95*) using the same equipment as for Au analysis. Ablation was done with a 85 µm diameter laser beam, a 10 Hz frequency and a fluence of 5 J.cm^{-2}. Gases used are He, Ar, and N with a flow rate of 0.3 L.min^{-1}, 0.85 L.min^{-1}, and 10 mL·min^{-1}, respectively. Elements measured include of Li^{7}, Si^{29}, Sc^{45}, V^{51}, Cr^{53}, Mn^{55}, Co^{59}, Ni^{60}, Cu^{63}, Zn^{66}, As^{75}, Rb^{85}, Sr^{88}, Y^{89}, Zr^{90}, Nb^{93}, Sn^{118}, Sb^{121}, Ba^{137}, La^{139}, Ce^{140}, Pr^{141}, Nd^{146}, Sm^{147}, Eu^{151}, Gd^{157}, Tb^{159}, Dy^{161}, Ho^{165}, Er^{167}, Tm^{169}, Yb^{172}, Lu^{175}, Hf^{178}, Ta^{181}, Tl^{205}, Pb^{208}, Bi^{209}, Th^{232}, U^{238}. Data reduction was

ARTICLE IN PRESS

done with IOLITE using also the 3DRS plugin (*96*). Pellets of the reference materials BCR-2, BHVO-1, BHVO-2, MRG-1 and RGM-1 have been used for testing accuracy and precision. Most elements are within 20% of the expected values for precision and accuracy in at least four standards out of five, except for Sb and Bi (Supplementary Data 4).

Sulfur and Carbon

Carbon and sulfur analyses were carried out at LERA using a Carbon–Sulfur Analyzer (CS-2000, Eltra). 150 mg rock powder samples were measured by solid-state infrared absorption. Standards steel and ductile iron from Eltra were used for instrument calibration and data quality check (Supplementary Data 5).

Mann-Withney U statistical test

The non-parametric Mann-Withney U statistical test is performed to determine Au mobility during prograde metamorphism as Au distribution in rocks is not normal (*20*). The null hypothesis of the test is defined as no difference in Au concentration between sample set 1 and sample set 2, with sample set 1 being the metamorphic protolith defined from Santorini and Ios Middle-CBU samples (n=21-32) and sample set 2 the samples from the Middle-CBU metamorphosed at different grade tested (n= 6-22, Table 2). The test is with an alpha level of 0.05 and is two tailed. Only samples from the Middle-CBU nappe are tested. Quartzite and marble samples are not used.

ARTICLE IN PRESS

References

1. K. H. Hattori, S. Guillot, Volcanic fronts form as a consequence of serpentinite dehydration in the forearc mantle wedge. *Geology* **31**, 525–528 (2003).
2. G. E. Bebout, S. C. Penniston-Dorland, Fluid and mass transfer at subduction interfaces—The field metamorphic record. *Lithos* **240**, 228–258 (2016).
3. H. Kawakatsu, S. Watada, Seismic evidence for deep-water transportation in the mantle. *Science (1979).* **316**, 1468–1471 (2007).
4. R. H. Sillitoe, A plate tectonic model for the origin of porphyry copper deposits. *Economic geology* **67**, 184–197 (1972).
5. R. J. Goldfarb, L. W. Snee, L. D. Miller, R. J. Newberry, Rapid dewatering of the crust deduced from ages of mesothermal gold deposits. *Nature* **354**, 296–298 (1991).

6. R. J. Goldfarb, D. I. Groves, Orogenic gold: Common or evolving fluid and metal sources through time. *Lithos* **233**, 2–26 (2015).

7. W. Sun, R. fang Huang, H. Li, Y. bin Hu, C. chan Zhang, S. jun Sun, L. peng Zhang, X. Ding, C. ying Li, R. E. Zartman, M. xing Ling, Porphyry deposits and oxidized magmas. *Ore Geol. Rev.* **65**, 97–131 (2015).

8. J. P. Richards, Magmatic to hydrothermal metal fluxes in convergent and collided margins. *Ore Geol. Rev.* **40**, 1–26 (2011).

9. M. D. Hannington, C. D. J. de Ronde, S. Petersen, "Sea-floor tectonics and submarine hydrothermal systems" (Society of Economic Geologists, 2005).

10. G. S. Pokrovski, M. A. Kokh, D. Guillaume, A. Y. Borisova, P. Gisquet, J.-L. Hazemann, E. Lahera, W. Del Net, O. Proux, D. Testemale, Sulfur radical species form gold deposits on Earth. *Proceedings of the National Academy of Sciences* **112**, 13484–13489 (2015).

11. B. I. A. McInnes, J. S. McBride, N. J. Evans, D. D. Lambert, A. S. Andrew, Osmium isotope constraints on ore metal recycling in subduction zones. *Science (1979).* **286**, 512–516 (1999).

12. D. I. Groves, M. Santosh, J. Deng, Q. Wang, L. Yang, L. Zhang, A holistic model for the origin of orogenic gold deposits and its implications for exploration. *Miner. Depos.*, 1–18 (2019).

13. S. Tassara, A. D. Rooney, J. J. Ague, D. Guido, M. Reich, F. Barra, C. Navarrete, Osmium isotopes fingerprint mantle controls on the genesis of an epithermal gold province. *Geology* **50**, 1291–1295 (2022).

14. R. J. Goldfarb, M. Santosh, The dilemma of the Jiaodong gold deposits: Are they unique? *Geoscience Frontiers* **5**, 139–153 (2014).

15. A. Boskabadi, I. K. Pitcairn, C. Broman, A. Boyce, D. A. H. Teagle, M. J. Cooper, M. K. Azer, R. J. Stern, F. H. Mohamed, J. Majka, Carbonate alteration of ophiolitic rocks in the Arabian–Nubian Shield of Egypt: sources and compositions of the

ARTICLE IN PRESS

carbonating fluid and implications for the formation of Au deposits. *Int. Geol. Rev.* **59**, 391–419 (2017).

16. J. E. Saunders, N. J. Pearson, S. Y. O'Reilly, W. L. Griffin, Gold in the mantle: A global assessment of abundance and redistribution processes. *Lithos* **322**, 376–391 (2018).

17. Z. Wang, H. Cheng, K. Zong, X. Geng, Y. Liu, J. Yang, F. Wu, H. Becker, S. Foley, C. Y. Wang, Metasomatized lithospheric mantle for Mesozoic giant gold deposits in the North China craton. *Geology* **48**, 169–173 (2020).

18. A. G. Tomkins, Windows of metamorphic sulfur liberation in the crust : Implications for gold deposit genesis. *Geochim. Cosmochim. Acta* **74**, 3246–3259 (2010).

19. I. K. Pitcairn, D. A. H. Teagle, D. Craw, G. R. Olivo, R. Kerrich, T. S. Brewer, Sources of metals and fluids in orogenic gold deposits: insights from the Otago and Alpone schists, New Zealand. *Economic Geology* **101**, 1525–1546 (2006).

20. I. K. Pitcairn, D. Craw, D. A. H. Teagle, Metabasalts as sources of metals in orogenic gold deposits. *Miner. Depos.* **50**, 373–390 (2015).

21. C. G. C. Patten, I. K. Pitcairn, F. Molnár, J. Kolb, G. Beaudoin, C. Guilmette, A. Peillod, Gold mobilization during metamorphic devolatilization of Archean and Paleoproterozoic metavolcanic rocks. *Geology* **48**, 1110–1114 (2020).

22. C. Spandler, C. Pirard, Element recycling from subducting slabs to arc crust: A review. *Lithos* **170**, 208–223 (2013).

23. J. Glodny, U. Ring, The Cycladic Blueschist Unit of the Hellenic subduction orogen: Protracted high-pressure metamorphism, decompression and reimbrication of a diachronous nappe stack. *Earth. Sci. Rev.* **224**, 103883 (2022).

24. D. P. Miller, H. R. Marschall, J. C. Schumacher, Metasomatic formation and petrology of blueschist-facies hybrid rocks from Syros (Greece): Implications for reactions at the slab–mantle interface. *Lithos* **107**, 53–67 (2009).

ARTICLE IN PRESS

ARTICLE IN PRESS

25. A. J. Kotowski, M. Cisneros, W. M. Behr, D. F. Stockli, K. Soukis, J. D. Barnes, D. Ortega-Arroyo, Subduction, underplating, and return flow recorded in the Cycladic Blueschist Unit exposed on Syros, Greece. *Tectonics* **41**, e2020TC006528 (2022).

26. A. Peillod, C. G. C. Patten, K. Drüppel, A. Beranoaguirre, A. Zeh, D. Gudelius, S. Hector, J. Majka, B. I. Kleine-Marshall, A. Karlson, Disruption of a high-pressure unit during exhumation: Example of the Cycladic Blueschist unit (Thera, Ios and Naxos islands, Greece). *Journal of Metamorphic Geology* **42**, 225–255 (2024).

27. U. Ring, H. Pantazides, J. Glodny, A. Skelton, Forced return flow deep in the subduction channel, Syros, Greece. *Tectonics* **39**, e2019TC005768 (2020).

28. L. Jolivet, J. P. Brun, Cenozoic geodynamic evolution of the Aegean. *International Journal of Earth Sciences* **99**, 109–138 (2010).

29. N. Skarpelis, A. Liati, The prevolcanic basement of Thera at Athinios: metamorphism, plutonism and mineralization. *Thera and the Aegean World III* **2**, 172–182 (1990).

30. S. N. Thomson, U. Ring, S. Brichau, J. Glodny, T. M. Will, Timing and nature of formation of the Ios metamorphic core complex, southern Cyclades, Greece. *Geological Society, London, Special Publications* **321**, 139–167 (2009).

31. A. Peillod, U. Ring, J. Glodny, A. Skelton, An Eocene/Oligocene blueschist-/greenschist facies P–T loop from the Cycladic Blueschist Unit on Naxos Island, Greece: Deformation-related re-equilibration vs. thermal relaxation. *Journal of Metamorphic Geology* **35**, 805–830 (2017).

32. F. Trotet, L. Jolivet, O. Vidal, Tectono-metamorphic evolution of Syros and Sifnos islands (Cyclades, Greese). *Tectonophysics* **338**, 179–206 (2001).

33. A. Skelton, A. Peillod, J. Glodny, I. Klonowska, C. Månbro, K. Lodin, U. Ring, Preservation of high pressure rocks coupled to rock composition and the absence of metamorphic fluids. *Journal of Metamorphic Geology* **37**, 359–381 (2019).

34. H. R. Marschall, T. Ludwig, R. Altherr, A. Kalt, S. Tonarini, Syros metasomatic tourmaline: evidence for very high-δ11B fluids in subduction zones. *Journal of Petrology* **47**, 1915–1942 (2006).

ARTICLE IN PRESS

35. G. Pe-Piper, D. J. W. Piper, “The South Aegean active volcanic arc: relationships between magmatism and tectonics” in *Developments in Volcanology* (Elsevier, 2005)vol. 7, pp. 113–133.

36. J. B. Walters, A. M. Cruz-Uribe, H. R. Marschall, Isotopic compositions of sulfides in exhumed high-pressure terranes: Implications for sulfur cycling in subduction zones. *Geochemistry, Geophysics, Geosystems* (2019).

37. C. G. C. Patten, F. Molnár, I. K. Pitcairn, J. Kolb, S. Mertanen, S. Hector, Multi-source and multi-stage metal mobilization during the tectonic evolution of the Central Lapland Greenstone Belt, Finland: implications for the formation of orogenic Au deposits. *Miner. Depos.* **58**, 461–488 (2023).

38. B. Mocek, Geochemical evidence for arc-type volcanism in the Aegean Sea: the blueschist unit of Siphnos, Cyclades (Greece). *Lithos* **57**, 263–289 (2001).

39. M. Keiter, C. Ballhaus, F. Tomaschek, *A New Geological Map of the Island of Syros (Aegean Sea, Greece): Implications for Lithostratigraphy and Structural History of the Cycladic Blueschist Unit* (Geological Society of America, 2011)vol. 481.

40. L. Fontboté, K. Kouzmanov, M. Chiaradia, G. S. Pokrovski, Sulfide minerals in hydrothermal deposits. *Elements* **13**, 97–103 (2017).

41. M. Edmonds, T. A. Mather, Volcanic sulfides and outgassing. *Elements* **13**, 105–110 (2017).

42. F. E. Jenner, H. S. C. O’Neill, R. J. Arculus, J. A. Mavrogenes, The magnetite crisis in the evolution of arc-related magmas and the initial concentration of Au, Ag and Cu. *Journal of Petrology* **51**, 2445–2464 (2010).

43. F. E. Jenner, R. J. Arculus, J. A. Mavrogenes, N. J. Dyriw, O. Nebel, E. H. Hauri, Chalcophile element systematics in volcanic glasses from the northwestern Lau Basin. *Geochemistry, Geophysics, Geosystems* **13** (2012).

44. C. G. C. Patten, I. K. Pitcairn, D. A. H. Teagle, Hydrothermal mobilisation of Au and other metals in supra-subduction oceanic crust: Insights from the Troodos ophiolite. *Ore Geol. Rev.* **86** (2017).

ARTICLE IN PRESS

ARTICLE IN PRESS

45. P. A. Brandl, M. Portnyagin, H. Zeppenfeld, F. J. Tepley, C. E. J. de Ronde, C. Timm, F. Hauff, D. Garbe-Schönberg, R. Bousquet, The origin of magmas and metals at the submarine Brothers volcano, Kermadec arc, New Zealand. *Economic Geology*, doi: https://doi.org/10.5382/econgeo.4973 (2022).

46. S. Hector, C. G. C. Patten, A. Beranoaguirre, P. Lanari, S. Kilias, P. Nomikou, A. Peillod, E. Eiche, J. Kolb, Magmatic evolution of the Kolumbo submarine volcano and its implication to seafloor massive sulfide formation. *Miner. Depos.*, 1–20 (2024).

47. C. G. C. Patten, I. K. Pitcairn, D. A. Teagle, M. Harris, Mobility of Au and related elements during the hydrothermal alteration of the oceanic crust: implications for the sources of metals in VMS deposits. *Miner. Depos.* **51**, 1–22 (2015).

48. J. B. Walters, A. M. Cruz-Uribe, H. R. Marschall, Sulfur loss from subducted altered oceanic crust and implications for mantle oxidation. *Geochem. Perspect. Lett.* (2020).

49. E. M. Schwarzenbach, M. J. Caddick, M. Petroff, B. C. Gill, E. H. G. Cooperdock, J. D. Barnes, Sulphur and carbon cycling in the subduction zone mélange. *Sci. Rep.* **8**, 1–11 (2018).

50. H. Barr, Preliminary fluid inclusion studies in a high-grade blueschist terrain, Syros, Greece. *Mineral. Mag.* **54**, 159–168 (1990).

51. B. I. Kleine, A. D. L. Skelton, B. Huet, I. K. Pitcairn, Preservation of blueschist-facies minerals along a shear zone by coupled metasomatism and fast-flowing CO2-bearing fluids. *Journal of Petrology* **55**, 1905–1939 (2014).

52. R. J. Goldfarb, I. Pitcairn, Orogenic gold: is a genetic association with magmatism realistic? *Miner. Depos.* **58**, 5–35 (2023).

53. E. Cannaò, N. Malaspina, From oceanic to continental subduction: Implications for the geochemical and redox evolution of the supra-subduction mantle. *Geosphere* **14**, 2311–2336 (2018).

54. R. R. Loucks, J. A. Mavrogenes, Gold solubility in supercritical hydrothermal brines measured in synthetic fluid inclusions. *Science (1979).* **284**, 2159–2163 (1999).

ARTICLE IN PRESS

ARTICLE IN PRESS

55. S. Farsang, Z. Zajacz, Sulfur species and gold transport in arc magmatic fluids. *Nat. Geosci.*, 1–7 (2024).

56. T. Hanyu, K. Shimizu, T. Ushikubo, J.-I. Kimura, Q. Chang, M. Hamada, M. Ito, H. Iwamori, T. Ishikawa, Tiny droplets of ocean island basalts unveil Earth’s deep chlorine cycle. *Nat. Commun.* **10**, 60 (2019).

57. A. E. Williams-Jones, R. J. Bowell, A. A. Migdisov, Gold in solution. *Elements* **5**, 281–287 (2009).

58. H. R. Marschall, J. C. Schumacher, Arc magmas sourced from mélange diapirs in subduction zones. *Nat. Geosci.* **5**, 862 (2012).

59. C. M. Breeding, J. J. Ague, M. Bröcker, Fluid–metasedimentary rock interactions in subduction-zone mélange: implications for the chemical composition of arc magmas. *Geology* **32**, 1041–1044 (2004).

60. J. B. Walters, A. M. Cruz-Uribe, H. R. Marschall, B. Boucher, The role of sulfides in the chalcophile and siderophile element budget of the subducted oceanic crust. *Geochim. Cosmochim. Acta* **304**, 191–215 (2021).

61. O. Plümper, T. John, Y. Y. Podladchikov, J. C. Vrijmoed, M. Scambelluri, Fluid escape from subduction zones controlled by channel-forming reactive porosity. *Nat. Geosci.* **10**, 150–156 (2017).

62. C. R. Wilson, M. Spiegelman, P. E. van Keken, B. R. Hacker, Fluid flow in subduction zones: The role of solid rheology and compaction pressure. *Earth Planet. Sci. Lett.* **401**, 261–274 (2014).

63. A. Menant, S. Angiboust, T. Gerya, Stress-driven fluid flow controls long-term megathrust strength and deep accretionary dynamics. *Sci. Rep.* **9**, 9714 (2019).

64. S. Kawano, I. Katayama, K. Okazaki, Permeability anisotropy of serpentinite and fluid pathways in a subduction zone. *Geology* **39**, 939–942 (2011).

65. E. Schettino, J. M. González-Jiménez, C. Marchesi, F. Palozza, I. F. Blanco-Quintero, F. Gervilla, R. Braga, C. J. Garrido, M. Fiorentini, Mantle-to-crust metal transfer by nanomelts. *Commun. Earth Environ.* **4**, 256 (2023).

ARTICLE IN PRESS

ARTICLE IN PRESS

66. A. Schaarschmidt, K. M. Haase, P. C. Voudouris, V. Melfos, R. Klemd, Migration of arc magmatism above mantle wedge diapirs with variable sediment contribution in the Aegean. *Geochemistry, Geophysics, Geosystems* **22**, e2020GC009565 (2021).

67. M. Klaver, G. Yogodzinski, C. Albert, M. Camejo-Harry, M. Elburg, K. Hoernle, C. Macpherson, G. Nowell, T. Rushmer, H. Williams, Widespread slab melting in modern subduction zones. *Earth Planet. Sci. Lett.* **626**, 118544 (2024).

68. S. J. Turner, C. H. Langmuir, An evaluation of five models of arc volcanism. *Journal of Petrology* **63**, egac010 (2022).

69. C. Timm, B. Davy, K. Haase, K. A. Hoernle, I. J. Graham, C. E. J. De Ronde, J. Woodhead, D. Bassett, F. Hauff, N. Mortimer, Subduction of the oceanic Hikurangi Plateau and its impact on the Kermadec arc. *Nat. Commun.* **5**, 4923 (2014).

70. E. A. Codillo, V. Le Roux, H. R. Marschall, Arc-like magmas generated by mélange-peridotite interaction in the mantle wedge. *Nat. Commun.* **9**, 2864 (2018).

71. S. G. Nielsen, H. R. Marschall, Geochemical evidence for mélange melting in global arcs. *Sci. Adv.* **3**, e1602402 (2017).

72. F. Wu, S. Turner, B. F. Schaefer, Mélange versus fluid and melt enrichment of subarc mantle: A novel test using barium isotopes in the Tonga-Kermadec arc. *Geology* **48**, 1053–1057 (2020).

73. J. L. Brown, S. C. Dyer, J. E. Mungall, A. G. Christy, D. J. Ellis, High-pressure Cu–Fe–S phase equilibria: some experimental and thermodynamic constraints on sulfides in subduction zones and the lithospheric mantle. *Journal of Petrology* **61**, egaa043 (2020).

74. E. M. Schwarzenbach, B. Dragovic, E. A. Codillo, L. Streicher, M. R. Scicchitano, U. Wiechert, F. Klein, H. R. Marschall, M. Scambelluri, Mobilization of isotopically heavy sulfur during serpentinite subduction. *Sci. Adv.* **10**, eadn0641 (2024).

75. S. J. Turner, I. Savov, T. Mather, R. Katz, D. R. Jones, D. Pyle, C.-J. de Hoog, S. Watt, Volcanic arc structure controlled by liquid focusing from the slab—evidence from boron isotopes and trace elements. (2024).

ARTICLE IN PRESS

ARTICLE IN PRESS

76. I. K. Pitcairn, N. Leventis, G. Beaudoin, S. Faure, C. Guilmette, B. Dubé, A metasedimentary source of gold in Archean orogenic gold deposits. *Geology* **49**, 862–866 (2021).

77. J. E. Mungall, J. M. Brenan, B. Godel, S. J. Barnes, F. Gaillard, Transport of metals and sulphur in magmas by flotation of sulphide melt on vapour bubbles. *Nat. Geosci.* **8**, 216–219 (2015).

78. O. Nadeau, A. E. Williams-Jones, J. Stix, Sulphide magma as a source of metals in arc-related magmatic hydrothermal ore fluids. *Nat. Geosci.* **3**, 501–505 (2010).

79. J. Chang, A. Audétat, T. Pettke, The gold content of mafic to felsic potassic magmas. *Nat. Commun.* **15**, 6988 (2024).

80. A. A. Georgatou, C. E. J. de Ronde, K. Kouzmanov, B. L. A. Charlier, D. Adams, Metals, volatiles, and lithostratigraphy of Brothers submarine volcano. *Geochemistry, Geophysics, Geosystems* **25**, e2024GC011716 (2024).

81. J.-W. Park, I. H. Campbell, M. Chiaradia, H. Hao, C.-T. Lee, Crustal magmatic controls on the formation of porphyry copper deposits. *Nat. Rev. Earth Environ.* **2**, 542–557 (2021).

82. J. P. Richards, The oxidation state, and sulfur and Cu contents of arc magmas: implications for metallogeny. *Lithos* **233**, 27–45 (2015).

83. A. Menant, L. Jolivet, J. Tuduri, C. Loiselet, G. Bertrand, L. Guillou-Frottier, 3D subduction dynamics: A first-order parameter of the transition from copper-to gold-rich deposits in the eastern Mediterranean region. *Ore Geol. Rev.* **94**, 118–135 (2018).

84. S. P. Kilias, J. Naden, I. Cheliotis, T. J. Shepherd, H. Constandinidou, J. Crossing, I. Simos, Epithermal gold mineralisation in the active Aegean volcanic arc: The Profitis Ilias deposit, Milos Island, Greece. *Miner. Depos.* **36**, 32–44 (2001).

85. S. Hector, Q. Ahmad, C. G. C. Patten, M. Chiaradia, P. Nomikou, S. Kilias, A. Peillod, S. Wagner, J. Kolb, Unravel subseafloor hydrothermal leaching and magmatic degassing during chimney formation at Kolumbo volcano. *Sci. Rep.* **15**, 14673 (2025).

ARTICLE IN PRESS

ARTICLE IN PRESS

86. P. Voudouris, C. Mavrogonatos, P. G. Spry, T. Baker, V. Melfos, R. Klemd, K. Haase, A. Repstock, A. Djiba, U. Bismayer, Porphyry and epithermal deposits in Greece: An overview, new discoveries, and mineralogical constraints on their genesis. *Ore Geol. Rev.* **107**, 654–691 (2019).

87. A. M. Rebaza, B. I. Holman, A. Mallik, E. H. G. Cooperdock, Mechanisms of mass transfer in sediment-rich mélanges in modern subduction zones. *J. Geophys. Res. Solid Earth* **130**, e2024JB030991 (2025).

88. B. Z. Klein, M. D. Behn, The impact of mélange formation on the rheology and H2O budget of the subduction zone interface, with implications for diapir nucleation. *Geophys. Res. Lett.* **52**, e2024GL113049 (2025).

89. U. Ring, J. Glodny, T. Will, S. Thomson, The Hellenic Subduction System: High-Pressure Metamorphism, Exhumation, Normal Faulting, and Large-Scale Extension. *Annu. Rev. Earth Planet. Sci.* **38**, 45–76 (2010).

90. A. Peillod, J. Majka, U. Ring, K. Drüppel, C. Patten, A. Karlsson, A. Włodek, E. Tehler, Differences in decompression of a high-pressure unit: A case study from the Cycladic Blueschist Unit on Naxos Island, Greece. *Lithos* **386**, 106043 (2021).

91. D. Müller, D. I. Groves, *Potassic Igneous Rocks and Associated Gold-Copper Mineralization* (Springer, 1997).

92. R. R. Large, J. B. Gemmell, H. Paulick, D. L. Huston, The alteration box plot: A simple approach to understanding the relationship between alteration mineralogy and lithogeochemistry associated with volcanic-hosted massive sulfide deposits. *Economic geology* **96**, 957–971 (2001).

93. D. Hasterok, M. Gard, C. M. B. Bishop, D. Kelsey, Chemical identification of metamorphic protoliths using machine learning methods. *Comput. Geosci.* **132**, 56–68 (2019).

94. C. G. C. Patten, A. Beranoaguirre, S. Hector, D. Gudelius, J. Kolb, E. Eiche, Improved whole rock low detection limit gold analysis by LA-ICP-MS utilizing pressed-powder-pellets. *Int. J. Mass Spectrom.* **488**, 117039 (2023).

ARTICLE IN PRESS

ARTICLE IN PRESS

95. D. Peters, T. Pettke, Evaluation of major to ultra trace element bulk rock chemical analysis of nanoparticulate pressed powder pellets by LA-ICP-MS. *Geostand. Geoanal. Res.* **41**, 5–28 (2017).

96. C. Paton, J. Hellstrom, B. Paul, J. Woodhead, J. Hergt, Iolite: Freeware for the visualisation and processing of mass spectrometric data. *J. Anal. At. Spectrom.* **26**, 2508–2518 (2011).

97. J. H. Crocket, H. Y. Kuo, Sources for gold, palladium and iridium in deep-sea sediments. *Geochim. Cosmochim. Acta* **43**, 831–842 (1979).

98. R. Arevalo, W. F. McDonough, Chemical variations and regional diversity observed in MORB. *Chem. Geol.* **271**, 70–85 (2010).

ARTICLE IN PRESS

Funding

C.G.C Patten and A. Peillod disclose support for the research of this work from the German Research Foundation (DFG PA 3523/7-1) and from the Bolin Centre for Climate Research (RA6_19_09_Peillod).

Acknowledgments

Author contributions:

Clifford G.C. Patten: conceptualization, field work, methodology, writing of original draft

Alexandre Peillod: conceptualization, field work, methodology, writing review and editing

Simon Hector: field work, methodology, writing review and editing

Barbara I. Kleine-Marshall: field work, writing review and editing

Aratz Beranoaguirre: methodology, writing review and editing

Antonin Bilau: methodology, writing review and editing

Kirsten Drüppel: field work, supervision, writing review and editing

Jesse B. Walters: field work, writing review and editing

Iain Pitcairn: writing review and editing

ARTICLE IN PRESS

Uwe Ring: field work, writing review and editing

Alasdair Skelton: field work, writing review and editing

Jochen Kolb: supervision, writing review and editing

Competing interests: The authors declare no competing interests.

Data and materials availability: All data are available in the main text or in the supplementary information and supplementary data. Supplementary data are accessible on the Zenodo public repository (DOI 10.5281/zenodo.19912888).

Sampling permissions: No sampling permission was required.

ARTICLE IN PRESS

Figure captions

Figure 1:

Figure 1. Geological overview of the Cyclades. a) Geological map of the Hellenic orogen, b) geological map of the Cyclades, c) Summary PT paths of the Middle- and Top-CBU nappes, d) cross section from A to A' through Santorini, Ios, Naxos and Syros. Modified from *26*.

Figure 2:

Figure 2. Box plots of gold content in metavolcanic and metasedimentary rocks from the Middle-CBU and Top-CBU nappes. Unmetamorphosed data are from fresh volcanic arc rocks (Supplementary Data 6), deep sea sediments (*97*) and sub-greenschist facies pelitic and psammitic rocks (*19*). Numbers next to box plots are medians values. Interquartile range are at 25-75 percentiles and the whiskers are at 1.5 the interquartile range. Solid lines connect median values and dashed lines connect average values. Quartzite and marble samples are not plotted.

Figure 3:

Figure 3. Box plots of LOI, S, As, and S contents from the Middle-CBU and Top-CBU nappes. A) Metavolcanic rocks and B) metasedimentary rocks. Box plots parameters are as in Figure 2.

Figure 4:

Figure 4. Gold distribution in volcanic rocks from different volcanic arcs and in metavolcanic rocks from the Middle-CBU nappe. A) Au vs MgO, B) Au vs V and C) Au/Cu vs V. Low Au content in Syros metavolcanic rocks is not associated with magmatic processes. SSZ arc analogues data from the Christiana-Santorini-Kolumbo volcanic field, Manus basin, Lau basin, Kermadec arc, Kamchatka arc, Troodos ophiolite and the Andean Southern Volcanic Zone (Supplementary Data 6).

Figure 5:

Figure 5: Box plots of Au/MgO, MgO, Au/V and V in metavolcanic rocks from the Middle-CBU from greenschist to eclogite metamorphic facies. Box plot parameters as in Figure 2.

Figure 6:

Figure 6. Slab components and arc magmatism Au fertility. a) Au concentration of Syros Top-CBU nappe mélange zone relative to $(La/Sm)_n$ vs. Ba/Th. Circle and triangle sizes indicate the Au concentration. Increase in $(La/Sm)_n$ is associated with terrigenous sedimentary rock input while increase in Ba/Th is associated with altered oceanic crust fluid and/or pelagic sediment inputs. Median Au concentrations of primitive volcanic rocks from different arcs are also shown (Supplementary Data 6). SB = Syros blocks, SM = Syros matrix, SMZ= Syros mélange zone, MORB = mid-ocean ridge basalt (*98*), AOC = altered oceanic crust, DM = depleted mantle, CSK = Christiana-Santorini-Kolumbo volcanic field, ASVZ = Andean South Volcanic Zone. Global mélange zone data (*58*) and Aegean volcanic arc data are also plotted (*66*). Modified from (*58*). b-d) Gold concentration in primitive volcanic rocks relative to $(La/Sm)_n$, Ba/Th and $(La/Sm)_n$/(Ba/Th). Volcanic arcs with strongly altered oceanic crust/pelagic sediment slab component show high Au content. Those with a strong terrigenous slab component show low Au content. Primitive volcanic rocks are defined as samples which have not sustained extensive magmatic differentiation, before magnetite, sulfide and/or volatile saturation. Correlation trends are plotted only from primitive volcanic rock data. Gold content in Syros blocks and matrix as well as in MORB are also plotted. See Supplementary Data 7.

ARTICLE IN PRESS

ARTICLE IN PRESS

Figure 7:

Figure 7. Model for the Au cycle in subduction zone. The main steps for Au mobilization in subduction zones are 1) Au mobilization from the slab during prograde HP-LT metamorphism at the upper blueschist/eclogite transition, 2) Au transport upwards along the slab-mantle interface towards the fore arc crust and/or pervasive mobilization in the mantle leading to local Au-rich metasomatized mantle, and 3) melting of the mélange zone with heterogenous Au distribution and contribution to arc magmatism. Hypothetical Au-rich deposit locations are also shown. Subduction zone architecture and relative positions of the islands representative of the CBU during the Eocene (*26*).

Figure 8:

Figure 8. Relationship between metamorphism, volcanism and Au-rich deposits formation in the Hellenic subduction system since 50 Ma. A) Aegean volcanic arc $(La/Sm)_n$ and Ba/Th and associated Au-rich ore deposits since the Eocene. Highest $(La/Sm)_n$ values are reached between 20-5 Ma when the volcanic arc records the signature of voluminous clastic material associated with the subduction of the external Hellenides (*66*). Gold-rich deposit during Aegean Arc migration formed mainly between 37-20 Ma in the Rhodopes and Biga areas (*83*). The Au-rich deposits associated with the Menderes metamorphic core complex, on the eastern margin of the Aegean arc, are not considered as they are related to slab-tear processes (*83*). B) Age of peak metamorphism of the various subducted units since the Eocene. Volcanic arc data from (*66*); 1 = Kassiteres, 2 = Maronia, 3 = Limnos, 4 = Samothraki, 5 = Ezine-Ayvacik, 6 = Lesbos, 7 = Skyros, 8 = Evia, 9 = Tinos, 10 = Serifos, 11 = Lavrion, 12 = Leptokaria, 13 = Aegina, 14 = Milos, 15 = Methana, 16 = CSK. Au-rich deposit data are from (*83*); a = Sahinli, b = Rosino, c = Ada Tepe, d = Sedefche district, e = Sapes-Kassiteres district, f = Kirazli, g = Perama Hill, h = Agi Dagi, i = Palea Kavala district, j = Skouries, k = Ovacik, l =Profitis Ilias. Au deposits for which the Au tonnage is unknown are plotted with a value of 1.

Figure 9:

Figure 9. Simplified tectonic evolution of the Hellenic subduction system and associated metamorphism, magmatism, and Au-rich deposit formation. Evolution of the Hellenic system is based on (*89*) and (*28*). Crustal material transfer through the mantle wedge can occur via diapirism or via slab melt/fluids. See text for details.

ARTICLE IN PRESS

ARTICLE IN PRESS

ARTICLE IN PRESS

Table 1:

Table 1. Gold content in the CBU

Metamorphic grade	Locality	n	Au (ng.g-1)			
			Middle-CBU nappe			
Metavolcanic rocks			Median	Average	Low.Q	Up.Q
Greenschist	Santorini	7	0.88	1.45	0.51	1.31
Lower Blueschist	Ios	14	0.84	1.30	0.57	1.93
Upper Blueschist	Naxos	7	0.94	1.74	0.56	1.55
Blueschist/Eclogite	Syros	14	0.29	0.33	0.23	0.40
Metasedimentary rocks						
Greenschist	Santorini	12	0.80	2.76	0.60	1.80
Lower Blueschist	Ios	21	1.12	2.52	0.71	2.83
Upper Blueschist	Naxos	22	1.69	22.70	0.71	3.98
Blueschist/Eclogite	Syros	6	0.29	0.45	0.11	0.50
			Top-CBU nappe			
Retrograde Eclo/GS	Syros blocks	14	0.86	1.71	0.62	2.26
Retrograde Eclo/GS	Syros matrix	10	0.57	2.14	0.41	3.53

Eclo/GS = eclogite to greenschist, Up.Q = upper quartile, Low. Q = lower quartile

ARTICLE IN PRESS

ARTICLE IN PRESS

Table 2:

Table 2. Mann Withney U tests

Sample set 1	n	Sample set 2	n	U value	Z value	P value	Null hypothesis
Metavolcanic rocks							
Metamorphic protolith	21	Middle CBU-Santorini	7	77.5	0.19	0.85	Not rejected
Metamorphic protolith	21	Middle CBU-Ios	14	143	-0.12	0.91	Not rejected
Metamorphic protolith	21	Middle CBU-Naxos	7	68	-0.27	0.79	Not rejected
Metamorphic protolith	21	Middle CBU-Syros	14	260	3.79	**1.58E-04**	**Rejected**
Metasedimentary rocks							
Metamorphic protolith	32	Middle CBU-Santorini	12	292	0.37	0.71	Not rejected
Metamorphic protolith	32	Middle CBU-Ios	21	279	0.26	0.80	Not rejected
Metamorphic protolith	32	Middle CBU-Naxos	22	313	-1.35	0.18	Not rejected
Metamorphic protolith	32	Middle CBU-Syros	6	184	2.38	**1.70E-02**	**Rejected**

ARTICLE IN PRESS

ARTICLE IN PRESS

Editorial summary:

Gold can be mobilized by fluids during blueschist–eclogite facies transitions in subduction zones with only partial retention of gold in the mélange zone, according to petrological and geochemical analyses of metamorphic rocks from the Aegean islands

Peer review information:
Communications Earth and Environment thanks the anonymous reviewers for their contribution to the peer review of this work. Primary Handling Editors: Santiago Tassara and Joe Aslin. A peer review file is available.

ARTICLE IN PRESS

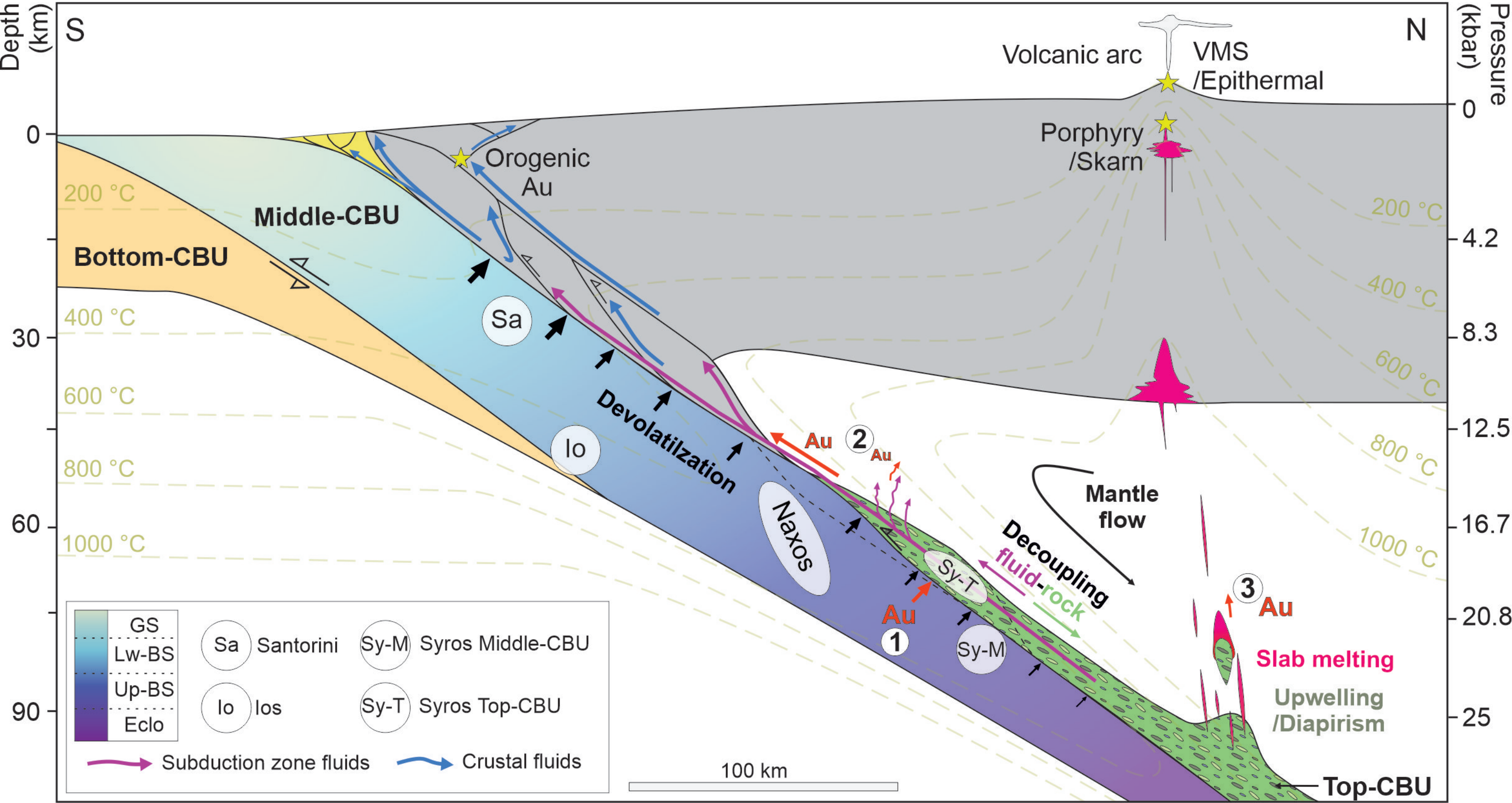
Depth (km)
Pressure (kbar)
S
N
0
30
60
90
0
4.2
8.3
12.5
16.7
20.8
25
Volcanic arc
VMS /Epithermal
Porphyry /Skarn
Orogenic Au
Middle-CBU
Bottom-CBU
200 °C
400 °C
600 °C
800 °C
1000 °C
Sa
Io
Naxos
Sy-T
Sy-M
Devolatilzation
Au
2
Au
Decoupling
fluid-rock
Mantle flow
1
Au
3
Au
Slab melting
Upwelling /Diapirism
Top-CBU
GS
Lw-BS
Up-BS
Eclo
Sa Santorini
Io Ios
Sy-M Syros Middle-CBU
Sy-T Syros Top-CBU
Subduction zone fluids
Crustal fluids
100 km

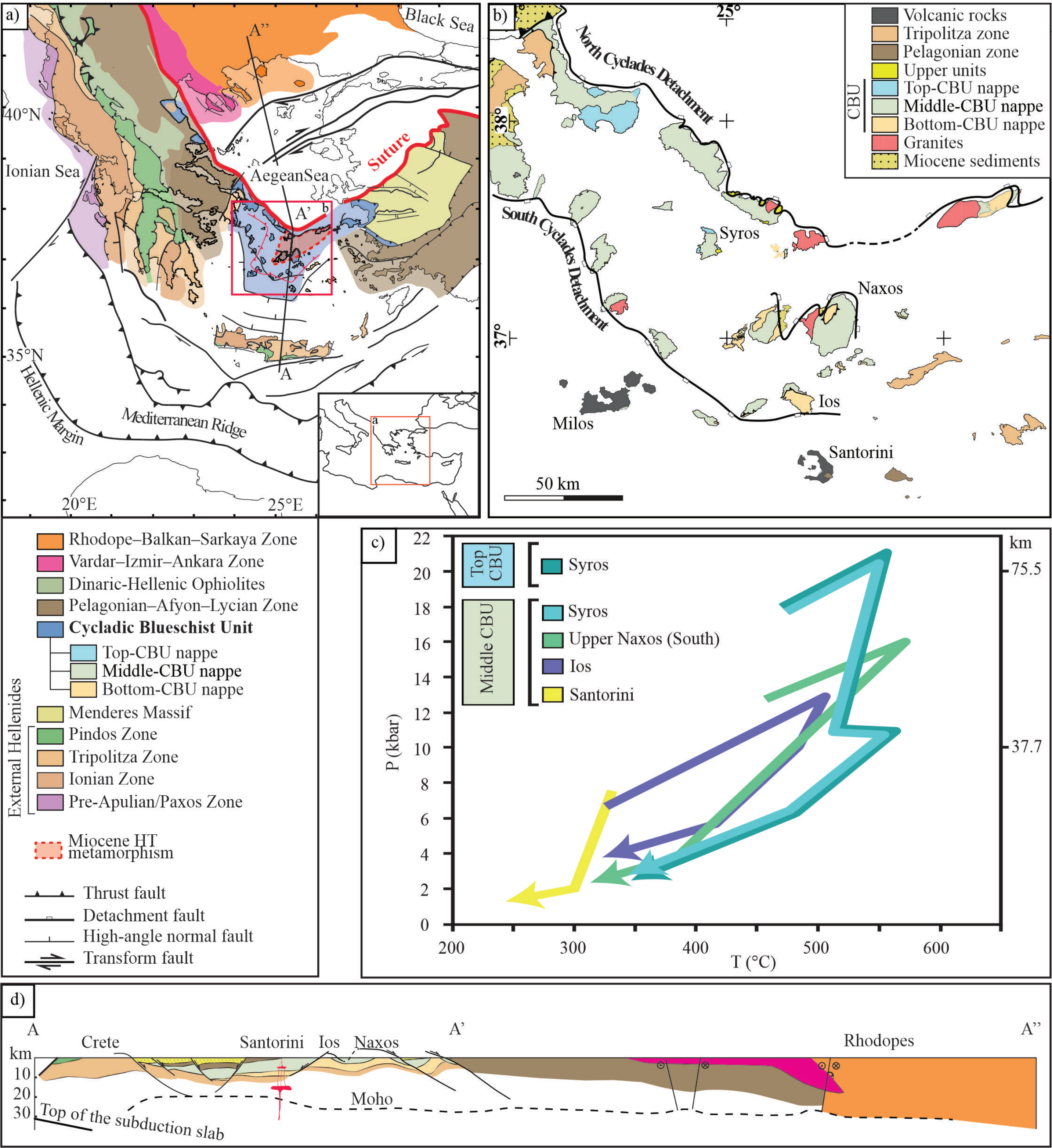
a)
Black Sea
A''
40°N
Ionian Sea
AegeanSea
Suture
A'
b
35°N
A
Hellenic Margin
Mediterranean Ridge
20°E
25°E
a
Rhodope–Balkan–Sarkaya Zone
Vardar–Izmir–Ankara Zone
Dinaric-Hellenic Ophiolites
Pelagonian–Afyon–Lycian Zone
Cycladic Blueschist Unit
Top-CBU nappe
Middle-CBU nappe
Bottom-CBU nappe
Menderes Massif
External Hellenides
Pindos Zone
Tripolitza Zone
Ionian Zone
Pre-Apulian/Paxos Zone
Miocene HT metamorphism
Thrust fault
Detachment fault
High-angle normal fault
Transform fault
b)
25°
38°
37°
North Cyclades Detachment
South Cyclades Detachment
Syros
Naxos
Ios
Milos
Santorini
50 km
Volcanic rocks
Tripolitza zone
Pelagonian zone
Upper units
CBU
Top-CBU nappe
Middle-CBU nappe
Bottom-CBU nappe
Granites
Miocene sediments
c)
Top CBU
Syros
Middle CBU
Syros
Upper Naxos (South)
Ios
Santorini
P (kbar)
22
20
18
16
14
12
10
8
6
4
2
0
km
75.5
37.7
200
300
400
500
600
T (°C)
d)
A
A'
A''
Crete
Santorini
Ios
Naxos
Rhodopes
km
10
20
30
Moho
Top of the subduction slab

ARTICLE IN PRESS

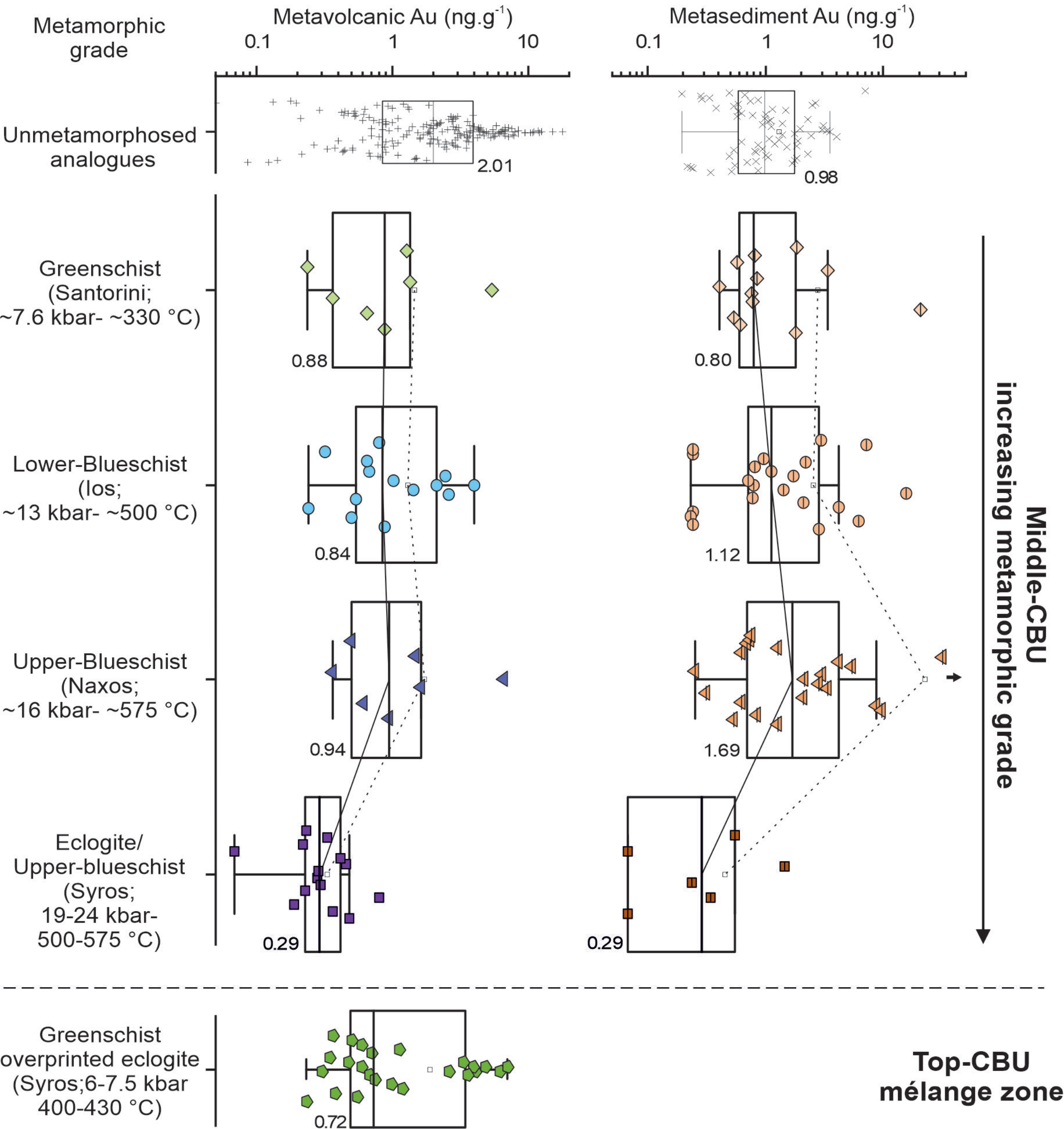

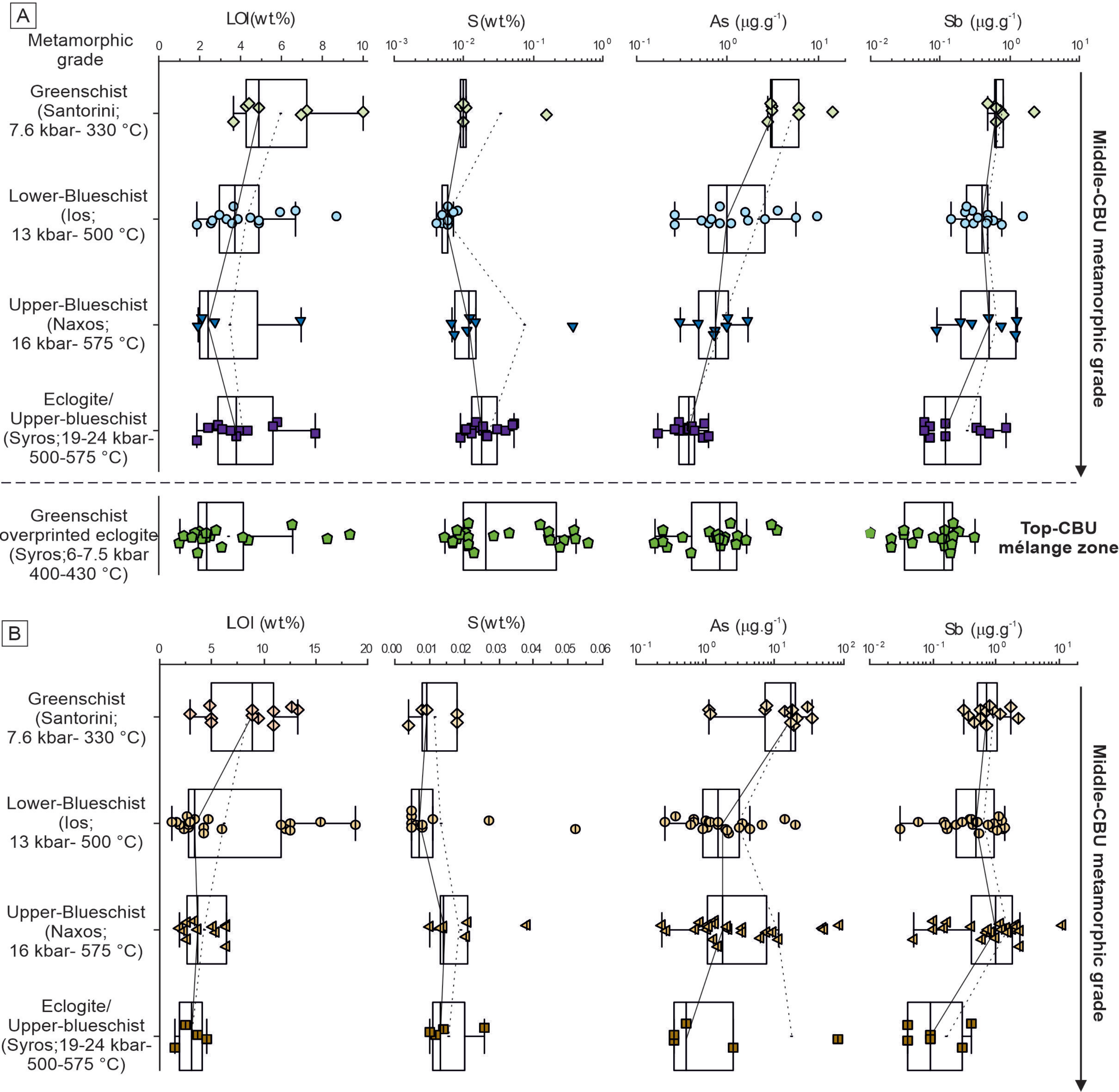
A
Metamorphic grade
LOI(wt%)
0 2 4 6 8 10
S(wt%)
10^{-3} 10^{-2} 10^{-1} 10^{0}
As ($\mu g.g^{-1}$)
10^{-1} 10^{0} 10^{1}
Sb ($\mu g.g^{-1}$)
10^{-2} 10^{-1} 10^{0} 10^{1}
Greenschist (Santorini; 7.6 kbar- 330 °C)
Lower-Blueschist (Ios; 13 kbar- 500 °C)
Upper-Blueschist (Naxos; 16 kbar- 575 °C)
Eclogite/ Upper-blueschist (Syros;19-24 kbar- 500-575 °C)
Middle-CBU metamorphic grade
Greenschist overprinted eclogite (Syros;6-7.5 kbar 400-430 °C)
Top-CBU mélange zone
B
LOI (wt%)
0 5 10 15 20
S(wt%)
0.00 0.01 0.02 0.03 0.04 0.05 0.06
As ($\mu g.g^{-1}$)
10^{-1} 10^{0} 10^{1} 10^{2}
Sb ($\mu g.g^{-1}$)
10^{-2} 10^{-1} 10^{0} 10^{1}
Greenschist (Santorini; 7.6 kbar- 330 °C)
Lower-Blueschist (Ios; 13 kbar- 500 °C)
Upper-Blueschist (Naxos; 16 kbar- 575 °C)
Eclogite/ Upper-blueschist (Syros;19-24 kbar- 500-575 °C)
Middle-CBU metamorphic grade

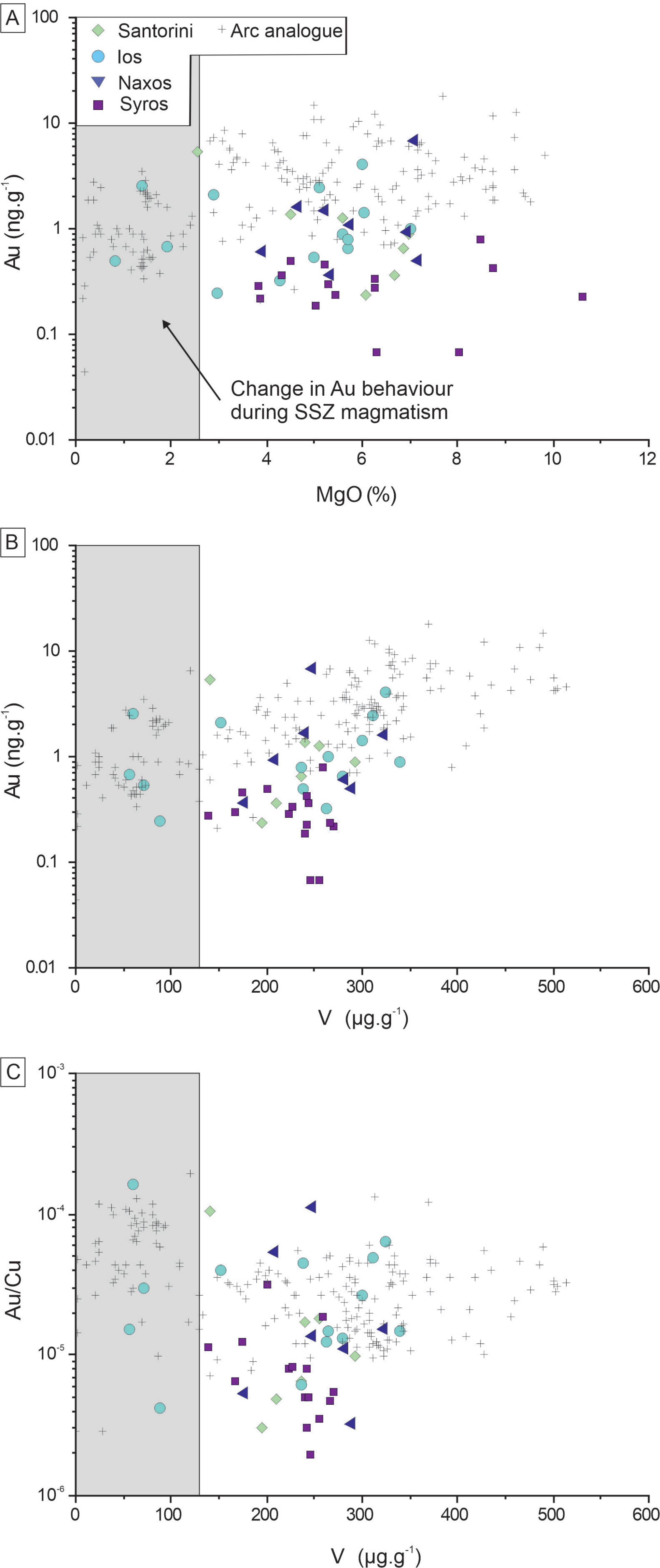
A
Santorini
Arc analogue
Ios
Naxos
Syros
Change in Au behaviour during SSZ magmatism
Au (ng.g^{-1})
100
10
1
0.1
0.01
0
2
4
6
8
10
12
MgO (%)
B
Au (ng.g^{-1})
V (µg.g^{-1})
0
100
200
300
400
500
600
C
Au/Cu
10^{-3}
10^{-4}
10^{-5}
10^{-6}
V (µg.g^{-1})

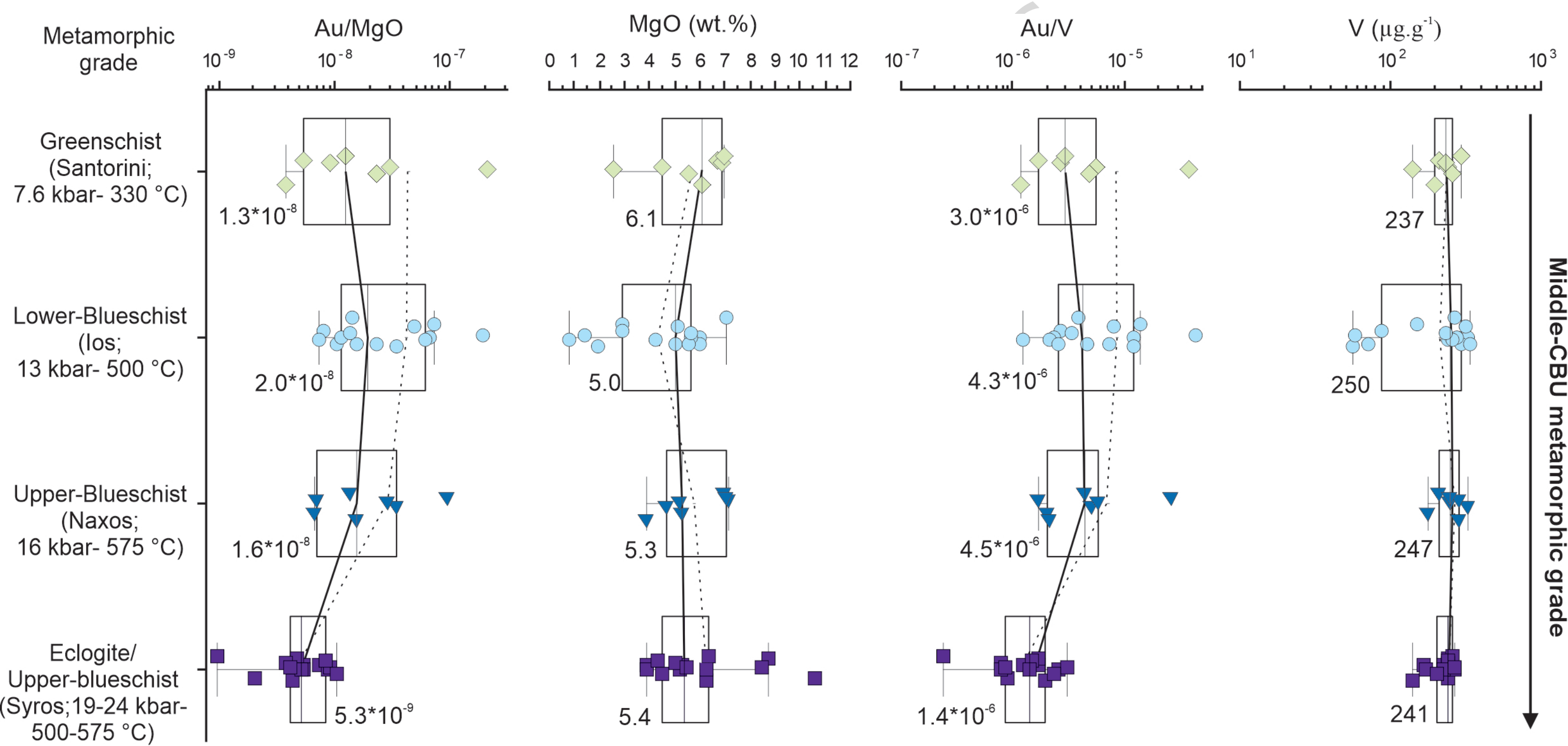
Metamorphic grade
Au/MgO
MgO (wt.%)
Au/V
V (µg.g-1)
10-9
10-8
10-7
0 1 2 3 4 5 6 7 8 9 10 11 12
10-7
10-6
10-5
101
102
103
Greenschist (Santorini; 7.6 kbar- 330 °C)
Lower-Blueschist (Ios; 13 kbar- 500 °C)
Upper-Blueschist (Naxos; 16 kbar- 575 °C)
Eclogite/ Upper-blueschist (Syros;19-24 kbar- 500-575 °C)
1.3*10-8
2.0*10-8
1.6*10-8
5.3*10-9
6.1
5.0
5.3
5.4
3.0*10-6
4.3*10-6
4.5*10-6
1.4*10-6
237
250
247
241
Middle-CBU metamorphic grade

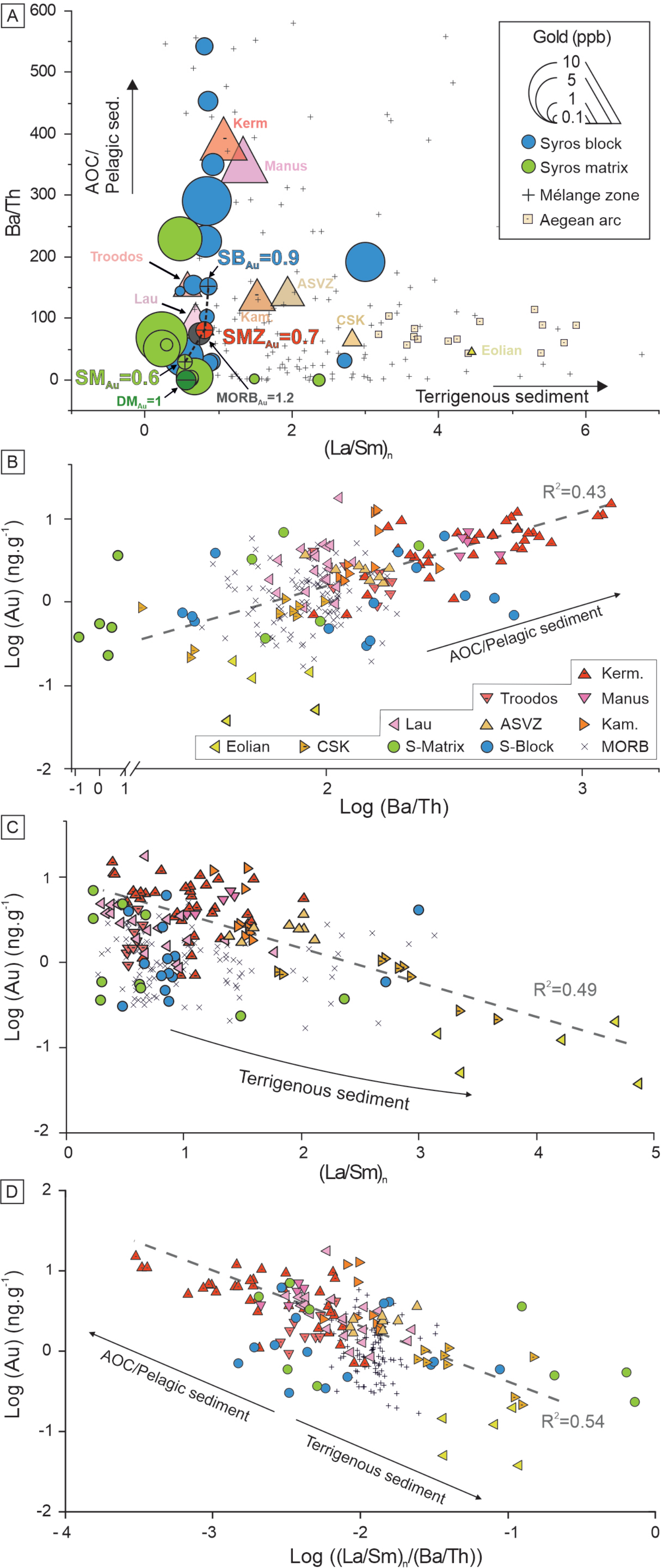
A
Ba/Th
600
500
400
300
200
100
0
(La/Sm)n
0
2
4
6
AOC/ Pelagic sed.
Terrigenous sediment
Kerm
Manus
Troodos
Lau
ASVZ
Kam
CSK
Eolian
SB$_{Au}$=0.9
SMZ$_{Au}$=0.7
SM$_{Au}$=0.6
DM$_{Au}$=1
MORB$_{Au}$=1.2
Gold (ppb)
10
5
1
0.1
Syros block
Syros matrix
Mélange zone
Aegean arc
B
Log (Au) (ng.g^{-1})
1
0
-1
-2
Log (Ba/Th)
-1
0
1
2
3
R^2=0.43
AOC/Pelagic sediment
Kerm.
Troodos
Manus
Lau
ASVZ
Kam.
Eolian
CSK
S-Matrix
S-Block
MORB
C
Log (Au) (ng.g^{-1})
1
0
-1
-2
(La/Sm)n
0
1
2
3
4
5
R^2=0.49
Terrigenous sediment
D
Log (Au) (ng.g^{-1})
2
1
0
-1
-2
Log ((La/Sm)n/(Ba/Th))
-4
-3
-2
-1
0
R^2=0.54
AOC/Pelagic sediment
Terrigenous sediment

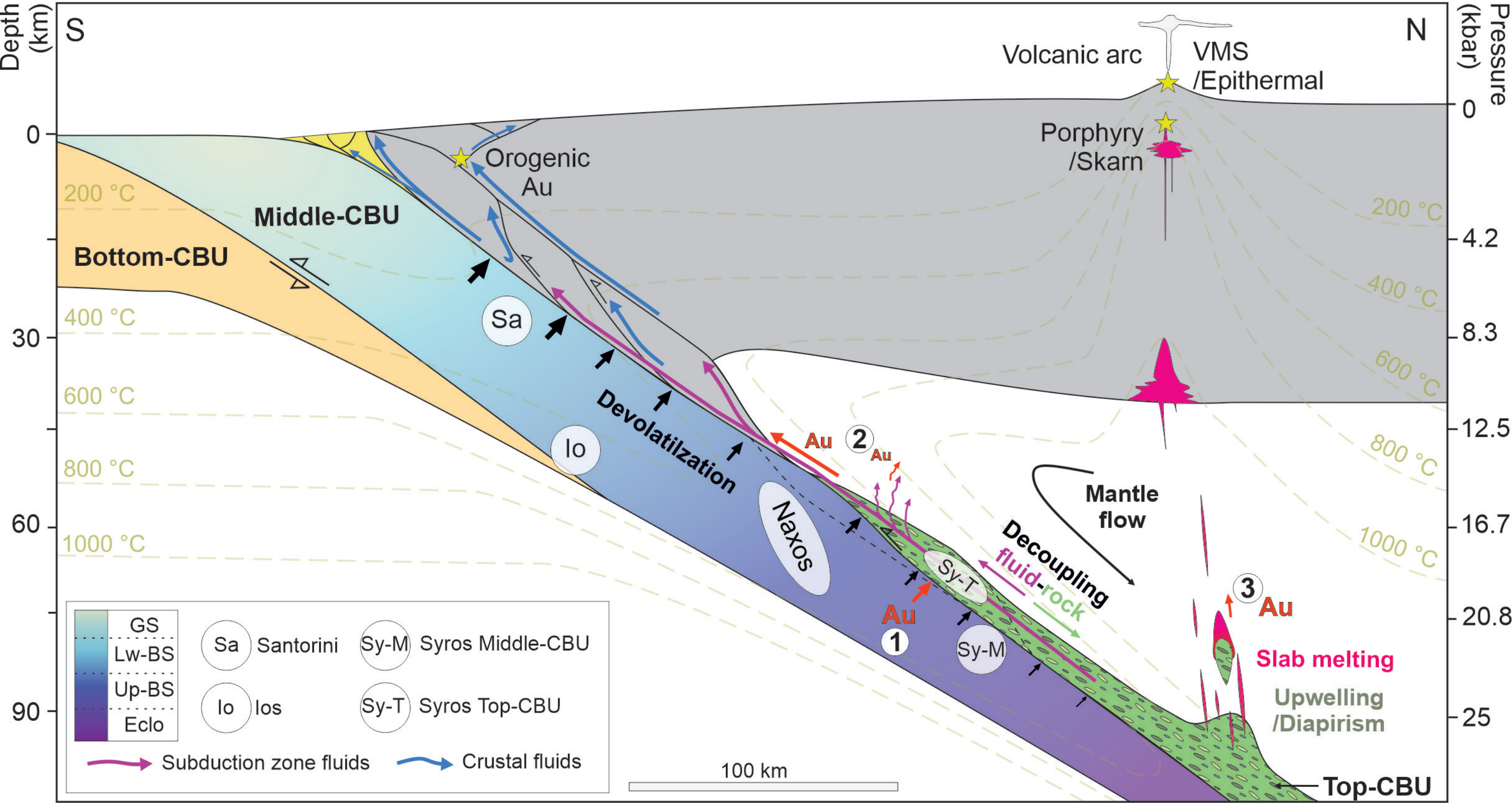
Depth (km)
S
N
Pressure (kbar)
0
30
60
90
0
4.2
8.3
12.5
16.7
20.8
25
Volcanic arc
VMS /Epithermal
Porphyry /Skarn
Orogenic Au
200 °C
400 °C
600 °C
800 °C
1000 °C
Middle-CBU
Bottom-CBU
Sa
Io
Naxos
Devolatilization
Au
2
Au
Mantle flow
Decoupling
fluid-rock
Sy-T
Sy-M
Au
1
3
Au
Slab melting
Upwelling /Diapirism
Top-CBU
GS
Lw-BS
Up-BS
Eclo
Sa Santorini
Io Ios
Sy-M Syros Middle-CBU
Sy-T Syros Top-CBU
Subduction zone fluids
Crustal fluids
100 km

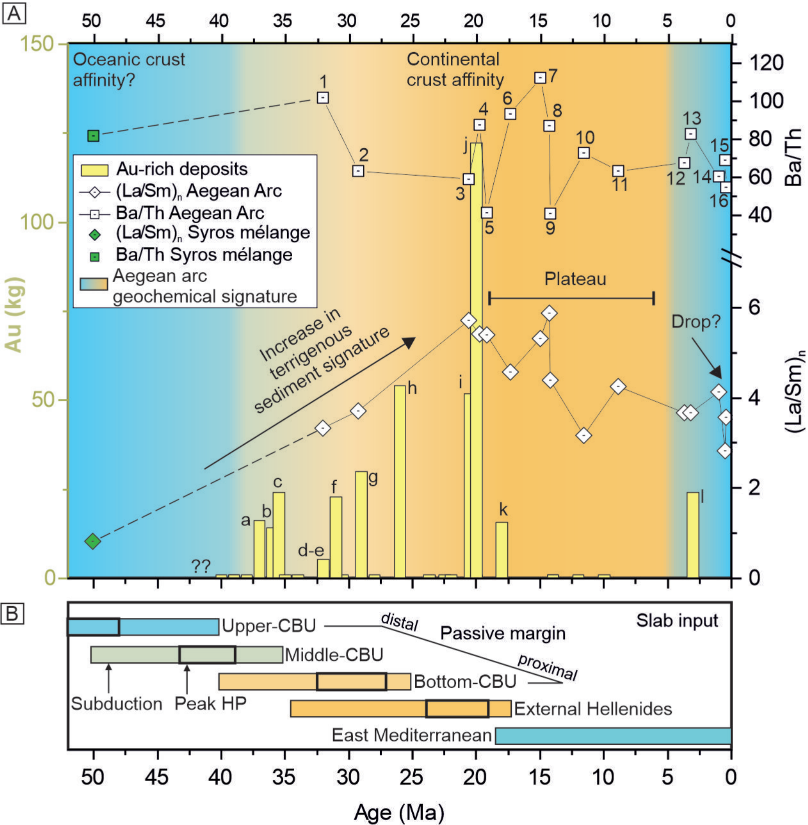
A
Oceanic crust affinity?
Continental crust affinity
Au-rich deposits
(La/Sm)$_n$ Aegean Arc
Ba/Th Aegean Arc
(La/Sm)$_n$ Syros mélange
Ba/Th Syros mélange
Aegean arc geochemical signature
Increase in terrigenous sediment signature
Plateau
Drop?
??
a
b
c
d-e
f
g
h
i
j
k
l
1
2
3
4
5
6
7
8
9
10
11
12
13
14
15
16
Au (kg)
150
100
50
0
Ba/Th
120
100
80
60
40
(La/Sm)$_n$
6
4
2
0
50
45
40
35
30
25
20
15
10
5
0
B
Slab input
Upper-CBU
distal
Passive margin
proximal
Middle-CBU
Bottom-CBU
External Hellenides
East Mediterranean
Subduction
Peak HP
Age (Ma)

ARTICLE IN PRESS